Article

Hidden-Charm Pentaquarks with Strangeness in a Chiral Quark Model

Gang Yang [1] , **Jialun Ping** [2] **and Jorge Segovia** [3,*]

1 Department of Physics, Zhejiang Normal University, Jinhua 321004, China; yanggang@zjnu.edu.cn
2 Department of Physics and Jiangsu Key Laboratory for Numerical Simulation of Large Scale Complex Systems, Nanjing Normal University, Nanjing 210023, China; jlping@njnu.edu.cn
3 Departamento de Sistemas Físicos, Químicos y Naturales, Universidad Pablo de Olavide, E-41013 Sevilla, Spain
* Correspondence: jsegovia@upo.es

Abstract: The LHCb collaboration has recently announced the discovery of two hidden-charm pentaquark states with strange quark content, $P_{cs}(4338)$ and $P_{cs}(4459)$; its analysis points towards having both hadrons' isospins equal to zero and spin-parity quantum numbers $\frac{1}{2}^-$ and $\frac{3}{2}^-$, respectively. Herein, we perform a systematical investigation of the $qqsc\bar{c}$ ($q = u, d$) system by means of a chiral quark model, along with a highly accurate computational method, the Gaussian expansion approach combined with the complex scaling technique. Baryon–meson configurations in both singlet- and hidden-color channels are considered. The $P_{cs}(4338)$ and $P_{cs}(4459)$ signals can be well identified as molecular bound states with dominant components $\Lambda J/\psi$ (60%) and $\Xi_c D$ (23%) for the lowest-energy case and $\Xi_c D^*$ (72%) for the highest-energy one. In addition, it seems that some narrow resonances can also be found in each allowed $I(J^P)$ channel in the energy region of 4.6–5.5 GeV, except for the $1(\frac{1}{2}^-)$ channel where a shallow bound state with dominant $\Xi_c^* D^*$ structure is obtained at 4673 MeV with binding energy $E_B = -3$ MeV. These exotic states are expected to be confirmed in future high-energy experiments.

Keywords: quantum chromodynamics; quark models

1. Introduction

During the past few years, some hadrons with five-quark content (pentaquarks) have been reported experimentally. In particular, the hidden-charm pentaquark candidate $P_c(4380)^+$ was the first to be announced by the LHCb collaboration in 2015 [1]. After that, three more pentaquark states, with equal minimum quark content of $qqqc\bar{c}$ ($q = u, d$), $P_c(4312)^+$, $P_c(4440)^+$ and $P_c(4457)^+$, were reported by the same collaboration in 2019 [2]. Additionally, progress in hidden-charm pentaquarks with strangeness has also been made by the LHCb collaboration since 2020. By using pp collision data, a $\Lambda J/\psi$ structure, which is labeled as $P_{cs}(4459)$, was reported in $\Xi_b^- \to J/\psi \Lambda K^-$ decays [3]. The mass and width of this hidden-charm pentaquark candidate with strange quark content are $4458.8 \pm 2.9^{+4.7}_{-1.1}$ MeV and $17.3 \pm 6.5^{+8.0}_{-5.7}$ MeV, respectively. In 2022, another strange pentaquark candidate, $P_{cs}(4338)$, was observed with high significance in $B^- \to J/\psi \Lambda \bar{p}$ decays [4]. Its experimental mass and width are $4338.2 \pm 0.7 \pm 0.4$ MeV and $7.0 \pm 1.2 \pm 1.3$ MeV. The spin-parity values of these two exotic states, $P_{cs}(4338)$ and $P_{cs}(4459)$, are preferably $\frac{1}{2}^-$ and $\frac{3}{2}^-$, respectively.

These facts have triggered an enormous amount of theoretical investigations; concerning the hidden-charm pentaquark candidates with strangeness, one may mention, for instance, the works performed within effective field theories [5–10], using QCD sum rules [11–15] or based on phenomenological quark models [16–23], generally establishing that the $P_{cs}(4338)$ state can be identified as a $\Xi_c \bar{D}^{(*)}$ molecular structure whereas the $P_{cs}(4459)$ state seems better for being a $\Xi_c^{(',*)} \bar{D}^{(*)}$ hadron molecule. However, mixed configurations [24,25],

compact structure analysis [26,27] and triangle singularities [28] could also explain the nature of the mentioned P_{cs} states. In addition, several additional exotic states in the hidden-charm pentaquark sector with strange quark content are theoretically proposed in Refs. [29–32]. In addition, the electromagnetic properties of the mentioned pentaquarks are calculated in Refs. [33–36]. The production and decay properties are also studied in Refs. [37–44].

Within the chiral quark model approach [45,46], supplemented by employing a highly accurate computational method on few-body problems, i.e., the combination of the Gaussian expansion method (GEM) [47] and the complex scaling method (CSM) [48], the S-wave hidden-charm pentaquarks with strangeness, having spin-parity $\frac{1}{2}^-$, $\frac{3}{2}^-$ and $\frac{5}{2}^-$, in the isoscalar and -vector sectors, are systematically investigated. This theoretical framework has already been successfully applied in various multiquark systems. A thorough review of our results can be found in Ref. [49] (see also related references cited therein); moreover, since then, we have continued studying charmonium- and bottomonium-like tetraquarks [50]; singly, doubly and fully heavy tetraquarks [51]; and hidden-charm and -bottom doubly and fully heavy pentaquarks [52]. Therefore, it is also a natural extension of our theoretical investigation to incorporate the analysis of pentaquark systems with strange quark content, beginning with the hidden-charm pentaquarks with strangeness motivated by the recently reported P_{cs} signals.

We arrange the present work in the following parts. In Section 2, the chiral quark model, pentaquark wave functions, GEM and CSM are briefly presented and discussed. Section 3 is devoted to the analysis and discussion of the obtained results. Finally, a summary is presented in Section 4.

2. Theoretical Framework

A thorough review of the theoretical formalism can be found in Ref. [49]. We shall then focus here on the most relevant features of the phenomenological model and the numerical method concerning the hidden-charm pentaquarks with strangeness $qqsc\bar{c}$ ($q = u$, d).

2.1. The Hamiltonian

The general form of the non-relativistic five-body Hamiltonian in the complex scaling method can be written as

$$H(\theta) = \sum_{i=1}^{5}\left(m_i + \frac{\vec{p}_i^{\,2}}{2m_i}\right) - T_{\text{CM}} + \sum_{j>i=1}^{5} V(\vec{r}_{ij}e^{i\theta}),\tag{1}$$

In Equation (1), T_{CM} is the center-of-mass kinetic energy and the two-body potential,

$$V(\vec{r}_{ij}e^{i\theta}) = V_{\text{CON}}(\vec{r}_{ij}e^{i\theta}) + V_{\text{OGE}}(\vec{r}_{ij}e^{i\theta}) + V_{\chi}(\vec{r}_{ij}e^{i\theta}),\tag{2}$$

which includes color-confining, one-gluon exchange and Goldstone–boson exchange interactions. The complex scaling method (CSM) allows us to simultaneously consider bound, resonance and scattering states, according to the so-called ABC theorem [53,54]. Within the CSM, the coordinates that describe relative motion between quarks are transformed with a complex rotation, $\vec{r} \to \vec{r}e^{i\theta}$; it should be understood that the same transformation applies to the conjugate momentum of the corresponding relative coordinate [48]. Accordingly, within the framework of complex range, the dynamics of a five-body system is determined by solving a complex scaled Schrödinger equation:

$$[H(\theta) - E(\theta)]\Psi_{JM_J}(\theta) = 0,\tag{3}$$

where the (complex) eigenvalue E can be assigned to three types of singularities: bound, resonance and scattering states. Particularly, bound states and resonances are independent of the rotated angle θ, with the first one placed on the real axis of the complex energy plane and the second one located above the continuum threshold with a total decay width given

by $\Gamma = -2\ \text{Im}(E)$. On the other hand, the scattering states depend on the rotated angle and follow the path marked by its associated continuum threshold. In particular, Figure 1 presents a schematic distribution of the complex energies according to Ref. [48].
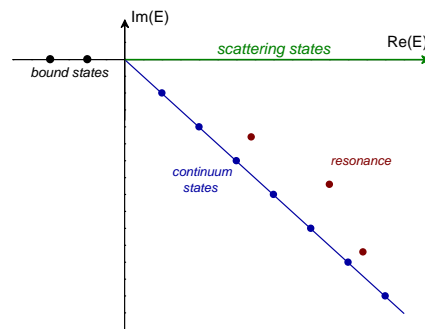

Figure 1. Schematic complex energy distribution in the single-channel two-body system.

Some details about the different potential terms in Equation (2) and their physical motivation come now. Firstly, color confinement should be encoded in the non-Abelian character of Quantum Chromodynamics (QCD). Some studies of QCD on a lattice have demonstrated that multi-gluon exchanges produce an attractive linearly rising potential proportional to the distance between infinitely heavy quarks [55]. However, the spontaneous creation of light–quark pairs from the QCD vacuum may give rise to a breakup of the color flux-tube at the same scale [55]. Our potential model tries to mimic these two phenomenological observations by the following expression in the complex scaling method:

$$V_{\text{CON}}(\vec{r}_{ij}e^{i\theta}) = \left[-a_c(1 - e^{-\mu_c r_{ij}e^{i\theta}}) + \Delta\right](\vec{\lambda}_i^c \cdot \vec{\lambda}_j^c),\tag{4}$$

where a_c and μ_c are model parameters and $\vec{\lambda}^c$ denotes the SU(3) color the Gell-Mann matrix. The potential of Equation (4) is linear at short inter-quark distances with an effective confinement strength $\sigma = -a_c\,\mu_c\,(\vec{\lambda}_i^c \cdot \vec{\lambda}_j^c)$, while it becomes constant at large distances, $V_{\text{thr}} = (\Delta - a_c)(\vec{\lambda}_i^c \cdot \vec{\lambda}_j^c)$.

The QCD perturbative effects are taken into account through one-gluon fluctuations around the instanton vacuum. Then, the different terms of the potential derived from the Lagrangian,

$$\mathcal{L}_{qqg} = i\sqrt{4\pi\alpha_s}\bar{\psi}\gamma_\mu G_c^\mu \lambda^c \psi,\tag{5}$$

contain central, tensor and spin–orbit contributions. For an *S*-wave pentaquark system, we consider herein only the central one, expressed also with a complex transformation $\vec{r} \to \vec{r}e^{i\theta}$,

$$V_{\text{OGE}}(\vec{r}_{ij}e^{i\theta}) = \frac{1}{4}\alpha_s(\vec{\lambda}_i^c \cdot \vec{\lambda}_j^c)\left[\frac{1}{r_{ij}e^{i\theta}} - \frac{1}{6m_im_j}(\vec{\sigma}_i \cdot \vec{\sigma}_j)\frac{e^{-r_{ij}e^{i\theta}/r_0(\mu)}}{r_{ij}e^{i\theta}r_0^2(\mu)}\right],\tag{6}$$

where m_i is the quark mass and $\vec{\sigma}$ denotes the Pauli matrices. The contact term has been regularized as follows:

$$\delta(\vec{r}_{ij}e^{i\theta}) \sim \frac{1}{4\pi r_0^2}\frac{e^{-r_{ij}e^{i\theta}/r_0}}{r_{ij}e^{i\theta}},\tag{7}$$

with $r_0(\mu_{ij}) = \hat{r}_0/\mu_{ij}$ depending on μ_{ij}, the reduced mass of a quark–(anti-)quark pair.

The wide energy range needed to provide a consistent description of mesons and baryons, from light to heavy quark sectors, requires an effective scale-dependent strong coupling constant [46]

$$\alpha_s(\mu_{ij}) = \frac{\alpha_0}{\ln\left(\frac{\mu_{ij}^2 + \mu_0^2}{\Lambda_0^2}\right)}, \tag{8}$$

where α_0, μ_0 and Λ_0 are model parameters.

Dynamical chiral symmetry breaking is the mechanism responsible for making light quarks, with very small current masses, acquire a dynamical, momentum-dependent mass $M(p)$, with $M(0) \approx 300\,\mathrm{MeV}$ for the u and d quarks, namely the constituent quark mass. To preserve chiral invariance of the QCD, Lagrangian new interaction terms, given by Goldstone boson exchanges, must appear. The central terms of the chiral quark–(anti-)quark interaction $V_\chi(\vec{r}_{ij}e^{i\theta})$ can be written as the following four parts:

$$V_\pi\left(\vec{r}_{ij}e^{i\theta}\right) = \frac{g_{ch}^2}{4\pi}\frac{m_\pi^2}{12m_im_j}\frac{\Lambda_\pi^2}{\Lambda_\pi^2 - m_\pi^2}m_\pi\left[Y(m_\pi r_{ij}e^{i\theta})\right.$$
$$\left. - \frac{\Lambda_\pi^3}{m_\pi^3}Y(\Lambda_\pi r_{ij}e^{i\theta})\right](\vec{\sigma}_i\cdot\vec{\sigma}_j)\sum_{a=1}^{3}(\vec{\lambda}_i^a\cdot\vec{\lambda}_j^a), \tag{9}$$

$$V_\sigma\left(\vec{r}_{ij}e^{i\theta}\right) = -\frac{g_{ch}^2}{4\pi}\frac{\Lambda_\sigma^2}{\Lambda_\sigma^2 - m_\sigma^2}m_\sigma\left[Y(m_\sigma r_{ij}e^{i\theta})\right.$$
$$\left. - \frac{\Lambda_\sigma}{m_\sigma}Y(\Lambda_\sigma r_{ij}e^{i\theta})\right], \tag{10}$$

$$V_K\left(\vec{r}_{ij}e^{i\theta}\right) = \frac{g_{ch}^2}{4\pi}\frac{m_K^2}{12m_im_j}\frac{\Lambda_K^2}{\Lambda_K^2 - m_K^2}m_K\left[Y(m_K r_{ij}e^{i\theta})\right.$$
$$\left. - \frac{\Lambda_K^3}{m_K^3}Y(\Lambda_K r_{ij}e^{i\theta})\right](\vec{\sigma}_i\cdot\vec{\sigma}_j)\sum_{a=4}^{7}(\vec{\lambda}_i^a\cdot\vec{\lambda}_j^a), \tag{11}$$

$$V_\eta\left(\vec{r}_{ij}e^{i\theta}\right) = \frac{g_{ch}^2}{4\pi}\frac{m_\eta^2}{12m_im_j}\frac{\Lambda_\eta^2}{\Lambda_\eta^2 - m_\eta^2}m_\eta\left[Y(m_\eta r_{ij}e^{i\theta})\right.$$
$$\left. - \frac{\Lambda_\eta^3}{m_\eta^3}Y(\Lambda_\eta r_{ij}e^{i\theta})\right](\vec{\sigma}_i\cdot\vec{\sigma}_j)\left[\cos\theta_p\left(\vec{\lambda}_i^8\cdot\vec{\lambda}_j^8\right)\right.$$
$$\left. - \sin\theta_p\right], \tag{12}$$

where $Y(x)$ is the Yukawa function defined by $Y(x) = e^{-x}/x$. The physical η meson is considered by introducing the angle θ_p. The $\vec{\lambda}^a$ is the SU(3) flavor Gell-Mann matrix. Taken from their experimental values, m_π, m_K and m_η are the masses of the SU(3) Goldstone bosons. The value of m_σ is determined through the partially conserved axial current (PCAC) relation $m_\sigma^2 \simeq m_\pi^2 + 4m_{u,d}^2$ [56]. Finally, the chiral coupling constant, g_{ch}, is determined from the πNN coupling constant through

$$\frac{g_{ch}^2}{4\pi} = \frac{9}{25}\frac{g_{\pi NN}^2}{4\pi}\frac{m_{u,d}^2}{m_N^2}, \tag{13}$$

which assumes that flavor SU(3) is an exact symmetry only broken by the different mass of the strange quark.

Finally, the chiral quark model parameters are summarized in Table 1. They have been fixed along the last two decades by thorough studies of hadron phenomenology such as meson [57,58] and baryon [59] spectra, hadron decays and reactions [60], coupling

between conventional hadrons and hadron–hadron thresholds [61] as well as molecular hadron–hadron formation [62].

Table 1. Quark model parameters.

Quark masses	$m_u = m_d$ (MeV)	313
	m_s (MeV)	555
	m_c (MeV)	1752
Goldstone bosons	$\Lambda_\pi = \Lambda_\sigma$ (fm^{-1})	4.20
	Λ_η (fm^{-1})	5.20
	$g_{ch}^2/(4\pi)$	0.54
	$\theta_P(^\circ)$	-15
Confinement	a_c (MeV)	430
	μ_c (fm^{-1})	0.70
	Δ (MeV)	181.10
OGE	α_0	2.118
	Λ_0 (fm^{-1})	0.113
	μ_0 (MeV)	36.976
	$\hat{r}_0$ (MeV fm)	28.170

2.2. The Wave Function

Three sets of configurations are generally needed for $qqsc\bar{c}$ ($q = u$, d) pentaquarks and are shown in Figure 2. Moreover, the anti-symmetry operator must be applied to each diagram as corresponding. Particularly, the anti-symmetry operator for the first configuration, panel (a) of Figure 2, is

$$\mathcal{A}_1 = \mathbb{1} - (1 \leftrightarrow 3) - (2 \leftrightarrow 3) \,. \tag{14}$$

This expression also holds for the second case, panel (b) of Figure 2b, viz., $\mathcal{A}_2 = \mathcal{A}_1$. Meanwhile, the anti-symmetry operator of panel (c) in Figure 2, where the two heavy quarks are arranged in each sub-cluster, reads

$$\mathcal{A}_3 = \mathbb{1} - (1 \leftrightarrow 2) - (1 \leftrightarrow 3) \,. \tag{15}$$

The pentaquark wave function is a product of four terms: color, flavor, spin and space wave functions. Firstly, concerning the color degree-of-freedom, there are richer structures in multiquark systems than in conventional hadrons. For instance, the color wave function of a pentaquark must be colorless, but the way of reaching this condition can be accomplished by either a color-singlet channel, hidden-color channel or both at the same time. The authors of Refs. [63,64] assert that it is enough to consider the color-singlet channel when all possible excited states of a system are included. However, a more economical and practical way is considering both. The color-singlet wave function is as follows:

$$\begin{aligned} \chi_1^{nc} = \frac{1}{\sqrt{18}} &(rgb - rbg + gbr - grb + brg - bgr) \\ &\times (\bar{r}r + \bar{g}g + \bar{b}b) \,, \end{aligned} \tag{16}$$

where $n = 1$, 2, 3 is a label for each of the three different configurations in Figure 2 (it is of the same meaning for spin, flavor and space wave functions). They are in a common form but with different quark sequences, namely 123;45, 125;43 and 235;41, respectively. In matrix element calculation, one should switch the remaining two cases with the first one in ascending order. Then, the hidden-color wave function is as follows:

$$\chi_k^{nc} = \frac{1}{\sqrt{8}} (\chi_{3,1}^{nk}\chi_{2,8} - \chi_{3,2}^{nk}\chi_{2,7} - \chi_{3,3}^{nk}\chi_{2,6} + \chi_{3,4}^{nk}\chi_{2,5}$$
$$+ \chi_{3,5}^{nk}\chi_{2,4} - \chi_{3,6}^{nk}\chi_{2,3} - \chi_{3,7}^{nk}\chi_{2,2} + \chi_{3,8}^{nk}\chi_{2,1}), \tag{17}$$

where $k = 2$, 3 is an index which stands for the symmetric and anti-symmetric configuration of two identical quarks in the 3-quark sub-cluster.
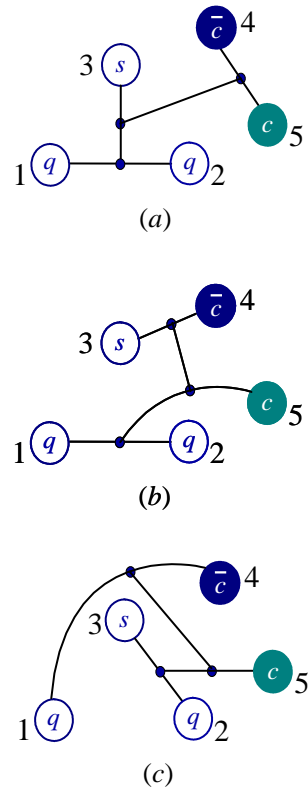
Figure 2. According to the SU(2) flavor symmetry, there are three kinds of baryon–meson configurations of the hidden-charm pentaquarks with strangeness. In particular, panel (**a**) shows the three-quark cluster with qqs content along with the $c\bar{c}$ pair, whereas panels (**b**,**c**) are of the $(qqc)(s\bar{c})$ and $(qsc)(q\bar{c})$ form, respectively. Note herein that we are considering interactions between quarks and (anti-)quarks that belong to different clusters, and it should be deduced from the discussion of the pentaquark wave function and in connection with the chiral potential presented in the text.

According to the SU(3) flavor symmetry in the isospin space, flavor wave functions for the sub-clusters mentioned above are given by:

$$B_{1,0}^{1+} = \frac{1}{\sqrt{12}} (2uds + 2dus - usd - dsu - sud - sdu), \tag{18}$$

$$B_{1,0}^{1-} = \frac{1}{\sqrt{2}} (usd - sud + dsu - sdu), \tag{19}$$

$$B_{1,0}^{1*} = \frac{1}{\sqrt{6}} (uds + dus + usd + dsu + sud + sdu), \tag{20}$$

$$B_{0,0}^{1+} = \frac{1}{\sqrt{2}} (usd - dsu + sud - sdu), \tag{21}$$

$$B_{0,0}^{1-} = \frac{1}{\sqrt{12}} (2uds - 2dus + usd - dsu - sud + sdu), \tag{22}$$

$$B_{1,0}^{2+} = \frac{1}{\sqrt{2}}(ud + du)c \,, \tag{23}$$

$$B_{0,0}^{2-} = \frac{1}{\sqrt{2}}(ud - du)c \,, \tag{24}$$

$$B_{\frac{1}{2},\frac{1}{2}}^{3\pm} = \frac{1}{\sqrt{2}}(us \pm su)c \,, \quad B_{\frac{1}{2},-\frac{1}{2}}^{3\pm} = \frac{1}{\sqrt{2}}(ds \pm sd)c \,, \tag{25}$$

$$M_{0,0}^{1} = \bar{c}c \,, \quad M_{0,0}^{2} = \bar{c}s \,, \tag{26}$$

$$M_{\frac{1}{2},\frac{1}{2}}^{3} = \bar{c}u \,, \quad M_{\frac{1}{2},-\frac{1}{2}}^{3} = \bar{c}d \,, \tag{27}$$

where the superscripts of cluster wave functions, *B* and *M*, stand for the assigned numbers of each of the three configurations and the subscripts refer to isospin (*I*) and its third component (M_I). Moreover, the symbols of $+(*)$ and $-$ in the wave function stand for a symmetry and anti-symmetry property of two quarks in the 3-quark sub-cluster. Consequently, flavor wave functions for the 5-quark system with isospin $I = 0$ and 1 are

$$\chi_{0,0}^{1f1}(5) = B_{0,0}^{1+}M_{0,0}^{1} \,, \quad \chi_{0,0}^{1f2}(5) = B_{0,0}^{1-}M_{0,0}^{1} \,, \tag{28}$$

$$\chi_{0,0}^{2f1}(5) = B_{0,0}^{2-}M_{0,0}^{2} \,, \tag{29}$$

$$\chi_{0,0}^{3f1}(5) = \frac{1}{\sqrt{2}}(B_{\frac{1}{2},\frac{1}{2}}^{3+}M_{\frac{1}{2},-\frac{1}{2}}^{3} - B_{\frac{1}{2},-\frac{1}{2}}^{3+}M_{\frac{1}{2},\frac{1}{2}}^{3}) \,, \tag{30}$$

$$\chi_{0,0}^{3f2}(5) = \frac{1}{\sqrt{2}}(B_{\frac{1}{2},\frac{1}{2}}^{3-}M_{\frac{1}{2},-\frac{1}{2}}^{3} - B_{\frac{1}{2},-\frac{1}{2}}^{3-}M_{\frac{1}{2},\frac{1}{2}}^{3}) \,, \tag{31}$$

$$\chi_{1,0}^{1f1}(5) = B_{1,0}^{1+}M_{0,0}^{1} \,, \quad \chi_{1,0}^{1f2}(5) = B_{1,0}^{1-}M_{0,0}^{1} \tag{32}$$

$$\chi_{1,0}^{1f3}(5) = B_{1,0}^{1*}M_{0,0}^{1} \,, \quad \chi_{1,0}^{2f1}(5) = B_{1,0}^{2+}M_{0,0}^{2} \tag{33}$$

$$\chi_{1,0}^{3f1}(5) = \frac{1}{\sqrt{2}}(B_{\frac{1}{2},\frac{1}{2}}^{3+}M_{\frac{1}{2},-\frac{1}{2}}^{3} + B_{\frac{1}{2},-\frac{1}{2}}^{3+}M_{\frac{1}{2},\frac{1}{2}}^{3}) \,, \tag{34}$$

$$\chi_{1,0}^{3f2}(5) = \frac{1}{\sqrt{2}}(B_{\frac{1}{2},\frac{1}{2}}^{3-}M_{\frac{1}{2},-\frac{1}{2}}^{3} + B_{\frac{1}{2},-\frac{1}{2}}^{3-}M_{\frac{1}{2},\frac{1}{2}}^{3}) \,, \tag{35}$$

where the third component of isospin is set to be zero without loss of generality because there is no interaction in the Hamiltonian that can distinguish such a component.

We are going to consider herein a 5-quark system with total spin ranging from 1/2 to 5/2. The Hamiltonian does not have any spin–orbit coupling-dependent interaction; therefore, the third component of spin is assumed to be equal to the total one without loss of generality. Then, the spin wave function is given by

$$\chi_{\frac{1}{2},\frac{1}{2}}^{n\sigma 1}(5) = \chi_{\frac{1}{2},\frac{1}{2}}^{n\sigma 1}(3)\chi_{00}^{\sigma} \,, \tag{36}$$

$$\chi_{\frac{1}{2},\frac{1}{2}}^{n\sigma 2}(5) = \chi_{\frac{1}{2},\frac{1}{2}}^{n\sigma 2}(3)\chi_{00}^{\sigma} \,, \tag{37}$$

$$\chi_{\frac{1}{2},\frac{1}{2}}^{n\sigma 3}(5) = \sqrt{\frac{1}{3}}\chi_{\frac{1}{2},\frac{1}{2}}^{n\sigma 1}(3)\chi_{10}^{\sigma} - \sqrt{\frac{2}{3}}\chi_{\frac{1}{2},-\frac{1}{2}}^{n\sigma 1}(3)\chi_{11}^{\sigma} \,, \tag{38}$$

$$\chi_{\frac{1}{2},\frac{1}{2}}^{n\sigma 4}(5) = \sqrt{\frac{1}{3}}\chi_{\frac{1}{2},\frac{1}{2}}^{n\sigma 2}(3)\chi_{10}^{\sigma} - \sqrt{\frac{2}{3}}\chi_{\frac{1}{2},-\frac{1}{2}}^{n\sigma 2}(3)\chi_{11}^{\sigma} \,, \tag{39}$$

$$\chi_{\frac{1}{2},\frac{1}{2}}^{n\sigma 5}(5) = \sqrt{\frac{1}{6}}\chi_{\frac{3}{2},-\frac{1}{2}}^{n\sigma}(3)\chi_{11}^{\sigma} - \sqrt{\frac{1}{3}}\chi_{\frac{3}{2},\frac{1}{2}}^{n\sigma}(3)\chi_{10}^{\sigma}$$

$$+ \sqrt{\frac{1}{2}}\chi_{\frac{3}{2},\frac{3}{2}}^{n\sigma}(3)\chi_{1-1}^{\sigma} \,, \tag{40}$$

for $S = 1/2$,

$$\chi^{n\sigma1}_{\frac{3}{2},\frac{3}{2}}(5) = \chi^{n\sigma1}_{\frac{1}{2},\frac{1}{2}}(3)\chi^{\sigma}_{11}\,, \tag{41}$$

$$\chi^{n\sigma2}_{\frac{3}{2},\frac{3}{2}}(5) = \chi^{n\sigma2}_{\frac{1}{2},\frac{1}{2}}(3)\chi^{\sigma}_{11}\,, \tag{42}$$

$$\chi^{n\sigma3}_{\frac{3}{2},\frac{3}{2}}(5) = \chi^{n\sigma}_{\frac{3}{2},\frac{3}{2}}(3)\chi^{\sigma}_{00}\,, \tag{43}$$

$$\chi^{n\sigma4}_{\frac{3}{2},\frac{3}{2}}(5) = \sqrt{\frac{3}{5}}\chi^{n\sigma}_{\frac{3}{2},\frac{3}{2}}(3)\chi^{\sigma}_{10} - \sqrt{\frac{2}{5}}\chi^{n\sigma}_{\frac{3}{2},\frac{1}{2}}(3)\chi^{\sigma}_{11}\,, \tag{44}$$

for $S = 3/2$, and

$$\chi^{n\sigma1}_{\frac{5}{2},\frac{5}{2}}(5) = \chi^{n\sigma}_{\frac{3}{2},\frac{3}{2}}(3)\chi^{\sigma}_{11}\,, \tag{45}$$

for $S = 5/2$. These expressions can be obtained easily through considering the 3-quark and quark–antiquark sub-clusters and using an SU(2) algebra.

Among the different methods for solving a complex Schrödinger-like 5-body bound state equation, we use the Rayleigh–Ritz variational principle, which is one of the most extended tools for solving eigenvalue problems due to its simplicity and flexibility. Then, the spatial wave function of a 5-quark system is written as follows:

$$\psi_{LM_L} = [[[\phi_{n_1l_1}(\vec{\rho}e^{i\theta})\phi_{n_2l_2}(\vec{\lambda}e^{i\theta})]_l\phi_{n_3l_3}(\vec{r}e^{i\theta})]_{l'}\phi_{n_4l_4}(\vec{R}e^{i\theta})]_{LM_L}\,. \tag{46}$$

Taking the first configuration of Figure 2a as an example, the internal Jacobi coordinates are defined as

$$\vec{\rho} = \vec{x}_1 - \vec{x}_2\,, \tag{47}$$

$$\vec{\lambda} = \vec{x}_3 - \left(\frac{m_1\vec{x}_1 + m_2\vec{x}_2}{m_1 + m_2}\right)\,, \tag{48}$$

$$\vec{r} = \vec{x}_4 - \vec{x}_5\,, \tag{49}$$

$$\vec{R} = \left(\frac{m_1\vec{x}_1 + m_2\vec{x}_2 + m_3\vec{x}_3}{m_1 + m_2 + m_3}\right) - \left(\frac{m_4\vec{x}_4 + m_5\vec{x}_5}{m_4 + m_5}\right)\,. \tag{50}$$

The other two configurations of Figure 2, i.e., panels (b) and (c), are very similar but consider a different arrangement of quark sequences. This choice is convenient because the center-of-mass kinetic term T_{CM} can be completely eliminated for a non-relativistic system, and it also allows us to extend the coordinates of relative motion between quarks into the complex scaling ground.

How to choose the basis on which to expand the genuine wave function of Equation (46) is important. Herein, by employing the Gaussian expansion method (GEM) [47], the spatial wave functions of each of the four relative motions are all expanded with Gaussian basis functions, whose sizes are taken in geometric progressions. This method was proven to be quite efficient in solving the bound state problem of multiquark systems [65–67], and details on how the geometric progression is fixed can be found in, e.g., Ref. [65]. Accordingly, the form of orbital wave functions ϕ in Equation (46) reads

$$\phi_{nlm}(\vec{r}e^{i\theta}) = N_{nl}(re^{i\theta})^l e^{-\nu_n(re^{i\theta})^2}Y_{lm}(\hat{r})\,. \tag{51}$$

Since only the S-wave states of $qqsc\bar{c}$ pentaquarks are investigated in this work, the spherical harmonic function is just a constant, viz., $Y_{00} = \sqrt{1/4\pi}$, and thus, no laborious Racah algebra is needed while computing matrix elements.

Finally, in order to fulfill the Pauli principle, the complete anti-symmetric complex wave function can be written as

$$
\begin{aligned}
\Psi_{JM_J,I} &= \sum_{i,j,k} c_{ijk} \Psi_{JM_J,I,i,j,k} \\
&= \sum_{i,j,k} \sum_{n=1}^{3} c_{ijk} \mathcal{A}_n \left[\left[\psi_{LM_L} \chi^{n\sigma_i}_{SM_S}(5) \right]_{JM_J} \chi^{nf_j}_I \chi^{nc}_k \right],
\end{aligned}
\tag{52}
$$

where $\mathcal{A}_n$ is the anti-symmetry operator of a 5-quark system, and its different expressions are shown in Equations (14) and (15). This is needed because we have constructed an anti-symmetric complex wave function for only two light quarks within the baryon sub-cluster, and the remaining quark of the system has been added to the wave function by simply considering the appropriate Clebsch–Gordan coefficients. Furthermore, the so-called expansion coefficients,

$$
|c_{ijk}|^2 = \langle \Psi_{JM_J,I,i,j,k} | \Psi_{JM_J,I} \rangle,
\tag{53}
$$

are determined, together with the pentaquark eigenenergy, by a generalized matrix eigenvalue problem.

Although the bases of different baryon–meson channels are not orthogonal to each other due to the anti-symmetry operator, and this is inevitable when working within a constituent quark model approach, the off-diagonal matrix elements are very small numerically and negligible when compared with the diagonal ones. Therefore, a quantitative analysis of the inter-quark distances, $r_{q\bar{q}}$, and a qualitative one of the dominant components, C_p, calculated as

$$
r_{q\bar{q}} = \sqrt{\langle \Psi_{JM_J,I} | r^2_{q\bar{q}} | \Psi_{JM_J,I} \rangle},
\tag{54}
$$

$$
C_p = \sum_{i,j,k \in C_p} \langle c^l_{ijk} \Psi_{JM_J,I,ijk} | c^r_{ijk} \Psi_{JM_J,I,ijk} \rangle,
\tag{55}
$$

where C_p is the component of one particular pentaquark channel and c^l_{ijk} and c^r_{ijk} are, respectively, the left and right generalized eigenvectors of the complete anti-symmetry complex wave function, can be performed in order to shed some light on the pentaquark's nature.

In the next section, where our results on hidden-charm pentaquarks with strangeness are discussed, we firstly study the systems by a real-range analysis, viz., the rotated angle θ is equal to $0°$. In this case, when a complete coupled-channel calculation of matrix diagonalization is performed, possible resonant states are embedded in the continuum. However, one can employ the CSM, with appropriate non-zero values of θ, to disentangle bound, resonance and scattering states in a complex energy plane. Accordingly, with the purpose of solving manageable eigenvalue problems, the artificial parameter of the rotated angle ranges from $0°$ to $6°$. Meanwhile, with the cooperation of real- and complex-range computations, available exotic states, which are firstly obtained within a complex-range analysis and then can be identified among continuum states according to their mass in a real-range calculation, are further investigated by analyzing their dominant quark arrangements, sizes and decay patterns.

3. Results

The lowest-lying and possible resonant states of S-wave $qqsc\bar{c}$ pentaquarks are investigated by taking into account three types of baryon–meson configurations, which include $(qqs)(\bar{c}c)$, $(qqc)(\bar{c}s)$ and $(qsc)(\bar{c}c)$, and they are shown in Figure 2. Therein, the angular momenta l_1, l_2, l_3 and l_4, which appear in Equation (46), are all equal to zero. Therefore, the total angular momentum, J, coincides with the total spin, S, and can take the values $1/2$, $3/2$ and $5/2$, respectively. The parity of the pentaquark system is then negative. Tables 2 and 3 list all allowed baryon–meson configurations of each $I(J^P)$ channel. In particular, channels

are indexed in the second column, and the third and fifth columns present the necessary basis combination in spin ($\chi_J^{n\sigma_i}$), flavor ($\chi_I^{nf_j}$) and color (χ_k^{nc}) degrees-of-freedom along with possible configurations ($n = 1, 2, 3$). Physical channels with color-singlet (labeled with the super-index 1) and color-octet (labeled with the super-index 8) configurations are listed in the fourth and sixth columns, respectively.

First of all, the lowest-lying $qqsc\bar{c}$ pentaquark in each channel is computed with a rotated angle $\theta = 0°$. The CSM is then employed in a fully coupled-channel calculation. Tables 4–14 summarize our results for the $qqsc\bar{c}$ system with spin-parity $J^P = \frac{1}{2}^-, \frac{3}{2}^-$ and $\frac{5}{2}^-$ and isospin $I = 0$ and 1. Figures 3–8 show the distribution of complex eigenenergies, and the obtained bound and resonance states are indicated inside colored orange circles. Finally, a summary of our most salient results is presented in Table 15.

In Tables 4, 6, 8, 10, 11 and 13, the baryon–meson configuration is listed in the first column, and the superscripts 1 and 8 stand for color-singlet and -octet states, respectively. The experimental threshold value of the baryon–meson channel is then listed in the parentheses. The lowest theoretical mass obtained in each channel is shown in the second column, and the binding energy is presented in the following one. A mixture of color-singlet and -octet configurations for each baryon–meson case is considered, and the coupled mass and binding energy are shown in the last column. The lowest-lying mass in coupled-channel calculation, which includes all-color-singlet, all-color-octet and a complete coupled-channel one, is indicated at the bottom of the tables. For the identified bound and resonance states, Tables 5, 7, 9, 12 and 14 list the sizes and probabilities of the different pentaquark configurations in their wave functions.

Table 2. All possible channels for $qqsc\bar{c}$ pentaquark systems with $J^P = 1/2^-$. Each channel is assigned an index in the second column, and it reflects a particular combination of spin ($\chi_J^{n\sigma_i}$), flavor ($\chi_I^{nf_j}$) and color (χ_k^{nc}) wave functions that are shown explicitly in the third and fifth columns. The baryon–meson configuration is listed in the fourth and last columns, and the superscripts 1 and 8 stand for color-singlet and -octet states, respectively.

J^P	Index	$I = 0$		$I = 1$	
		$\chi_J^{n\sigma_i}; \chi_I^{nf_j}; \chi_k^{nc};$ $[i; j; k; n]$	Channel	$\chi_J^{n\sigma_i}; \chi_I^{nf_j}; \chi_k^{nc};$ $[i; j; k; n]$	Channel
$\frac{1}{2}^-$	1	$[1, 2; 1, 2; 1; 1]$	$(\Lambda\eta_c)^1$	$[1, 2; 1, 2; 1; 1]$	$(\Sigma\eta_c)^1$
	2	$[2; 1; 1; 2]$	$(\Lambda_c D_s)^1$	$[3, 4; 1, 2; 1; 1]$	$(\Sigma J/\psi)^1$
	3	$[1; 1; 1; 3]$	$(\Xi_c' D)^1$	$[5; 3; 1; 1]$	$(\Sigma^* J/\psi)^1$
	4	$[2; 2; 1; 3]$	$(\Xi_c D)^1$	$[1; 1; 1; 2]$	$(\Sigma_c D_s)^1$
	5	$[3, 4; 1, 2; 1; 1]$	$(\Lambda J/\psi)^1$	$[3; 1; 1; 2]$	$(\Sigma_c D_s^*)^1$
	6	$[4; 1; 1; 2]$	$(\Lambda_c D_s^*)^1$	$[5; 1; 1; 2]$	$(\Sigma_c^* D_s^*)^1$
	7	$[3; 1; 1; 3]$	$(\Xi_c' D^*)^1$	$[1; 1; 1; 3]$	$(\Xi_c' D)^1$
	8	$[4; 2; 1; 3]$	$(\Xi_c D^*)^1$	$[2; 2; 1; 3]$	$(\Xi_c D)^1$
	9	$[5; 1; 1; 3]$	$(\Xi_c^* D^*)^1$	$[3; 1; 1; 3]$	$(\Xi_c' D^*)^1$
	10	$[1, 2; 1, 2; 2, 3; 1]$	$(\Lambda\eta_c)^8$	$[4; 2; 1; 3]$	$(\Xi_c D^*)^1$
	11	$[1, 2; 1; 2, 3; 2]$	$(\Lambda_c D_s)^8$	$[5; 1; 1; 3]$	$(\Xi_c^* D^*)^1$
	12	$[1, 2; 1; 2, 3; 3]$	$(\Xi_c' D)^8$	$[1, 2; 1, 2; 2, 3; 1]$	$(\Sigma\eta_c)^8$
	13	$[1, 2; 2; 2, 3; 3]$	$(\Xi_c D)^8$	$[3, 4; 1, 2; 2, 3; 1]$	$(\Sigma J/\psi)^8$
	14	$[3, 4; 1, 2; 2, 3; 1]$	$(\Lambda J/\psi)^8$	$[5; 1, 2; 2, 3; 1]$	$(\Sigma^* J/\psi)^8$
	15	$[3, 4; 1; 2, 3; 2]$	$(\Lambda_c D_s^*)^8$	$[1, 2; 1; 2, 3; 2]$	$(\Sigma_c D_s)^8$
	16	$[3, 4; 1; 2, 3; 3]$	$(\Xi_c' D^*)^8$	$[3, 4; 1; 2, 3; 2]$	$(\Sigma_c D_s^*)^8$
	17	$[3, 4; 2; 2, 3; 3]$	$(\Xi_c D^*)^8$	$[5; 1; 3; 2]$	$(\Sigma_c^* D_s^*)^8$
	18	$[5; 1, 2; 2, 3; 3]$	$(\Xi_c^* D^*)^8$	$[1, 2; 1; 2, 3; 3]$	$(\Xi_c' D)^8$
	19			$[1, 2; 2; 2, 3; 3]$	$(\Xi_c D)^8$
	20			$[3, 4; 1; 2, 3; 3]$	$(\Xi_c' D^*)^8$
	21			$[3, 4; 2; 2, 3; 3]$	$(\Xi_c D^*)^8$
	22			$[5; 1, 2; 2, 3; 3]$	$(\Xi_c^* D^*)^8$

Table 3. All possible channels for $qqsc\bar{c}$ pentaquark systems with $3/2^-$ and $5/2^-$. Columns are similarly organized as those in Table 2.

J^P	Index	$\chi_J^{n\sigma_i}; \chi_I^{nf_j}; \chi_k^{nc};$ $[i; j; k; n]$ (I=0)	Channel (I=0)	$\chi_J^{n\sigma_i}; \chi_I^{nf_j}; \chi_k^{nc};$ $[i; j; k; n]$ (I=1)	Channel (I=1)
$\frac{3}{2}^-$	1	$[1,2; 1,2; 1; 1]$	$(\Lambda J/\psi)^1$	$[1,2; 1,2; 1; 1]$	$(\Sigma J/\psi)^1$
	2	$[2; 1; 1; 2]$	$(\Lambda_c D_s^*)^1$	$[3; 3; 1; 1]$	$(\Sigma^*\eta_c)^1$
	3	$[1; 1; 1; 3]$	$(\Xi_c' D^*)^1$	$[4; 3; 1; 1]$	$(\Sigma^* J/\psi)^1$
	4	$[2; 2; 1; 3]$	$(\Xi_c D^*)^1$	$[1; 1; 1; 2]$	$(\Sigma_c D_s^*)^1$
	5	$[3; 1; 1; 3]$	$(\Xi_c^* D)^1$	$[3; 1; 1; 2]$	$(\Sigma_c^* D_s)^1$
	6	$[4; 1; 1; 3]$	$(\Xi_c^* D^*)^1$	$[4; 1; 1; 2]$	$(\Sigma_c^* D_s^*)^1$
	7	$[1,2; 1,2; 2,3; 1]$	$(\Lambda J/\psi)^8$	$[1; 1; 1; 3]$	$(\Xi_c' D^*)^1$
	8	$[1,2; 1; 2,3; 2]$	$(\Lambda_c D_s^*)^8$	$[2; 2; 1; 3]$	$(\Xi_c D^*)^1$
	9	$[1,2; 1; 2,3; 3]$	$(\Xi_c' D^*)^8$	$[3; 1; 1; 3]$	$(\Xi_c^* D)^1$
	10	$[1,2; 2; 2,3; 3]$	$(\Xi_c D^*)^8$	$[4; 1; 1; 3]$	$(\Xi_c^* D^*)^1$
	11	$[3; 1,2; 2,3; 3]$	$(\Xi_c^* D)^8$	$[1,2; 1,2; 2,3; 1]$	$(\Sigma J/\psi)^8$
	12	$[4; 1,2; 2,3; 3]$	$(\Xi_c^* D^*)^8$	$[3; 1,2; 2,3; 1]$	$(\Sigma^*\eta_c)^8$
	13			$[4; 1,2; 2,3; 1]$	$(\Sigma^* J/\psi)^8$
	14			$[1,2; 1; 2,3; 2]$	$(\Sigma_c D_s^*)^8$
	15			$[3; 1; 3; 2]$	$(\Sigma_c^* D_s)^8$
	16			$[4; 1; 3; 2]$	$(\Sigma_c^* D_s^*)^8$
	17			$[1,2; 1; 2,3; 3]$	$(\Xi_c' D^*)^8$
	18			$[1,2; 2; 2,3; 3]$	$(\Xi_c D^*)^8$
	19			$[3; 1,2; 2,3; 3]$	$(\Xi_c^* D)^8$
	20			$[4; 1,2; 2,3; 3]$	$(\Xi_c^* D^*)^8$
$\frac{5}{2}^-$	1	$[1; 1; 1; 3]$	$(\Xi_c^* D^*)^1$	$[1; 3; 1; 1]$	$(\Sigma^* J/\psi)^1$
	2	$[1; 1,2; 2,3; 3]$	$(\Xi_c^* D^*)^8$	$[1; 1; 1; 2]$	$(\Sigma_c^* D_s^*)^1$
	3			$[1; 1; 1; 3]$	$(\Xi_c^* D^*)^1$
	4			$[1; 1,2; 2,3; 1]$	$(\Sigma^* J/\psi)^8$
	5			$[1; 1; 3; 2]$	$(\Sigma_c^* D_s^*)^8$
	6			$[1; 1,2; 2,3; 3]$	$(\Xi_c^* D^*)^8$

We proceed now to describing our theoretical findings in detail. However, two comments are in order here. Firstly, there are two sources of theoretical uncertainties in our results: one is intrinsic to the numerical algorithm and the other is related to the way the model parameters are fixed. The numerical error is negligible and, as mentioned in the text, the model parameters are adjusted to reproduce a certain number of hadron observables within a determinate range of agreement with the experiment. It is therefore difficult to assign an error to these parameters and consequently to the quantities calculated using them. Secondly, it has been demonstrated that, given a multiquark system, the lowest-energy state in the spectrum corresponds to one of the possible meson(s) plus baryon(s) configurations. Therefore, for the case at hand, the lowest-mass state should correspond to a particular meson–baryon configuration, $(qqq) - (q\bar{q})$, and not to other kinds of arrangements such as $(qq)(qq)\bar{q}$, $(qq\bar{q})(qq)$, $(qqq\bar{q})q$, etc. Since we are interested in finding the lowest-energy states supported by the $qqsc\bar{c}$ pentaquark system, under a particular dynamical Hamiltonian, we have excluded in our study other configurations beyond meson–baryon ones with the purpose of obtaining a manageable Hamiltonian matrix to work with. In addition, there may be coupling effects among all configurations, included the ignored ones, but these are usually weak when treating different arrangements of quarks.

Table 4. The lowest-lying $qqsc\bar{c}$ pentaquark states with $I(J^P) = 0(\frac{1}{2}^-)$ calculated in a real-range formulation of the potential model. The baryon–meson configuration is listed in the first column, and the superscripts 1 and 8 stand for color-singlet and -octet states, respectively. The experimental threshold value of the baryon–meson channel is listed in the parentheses. The lowest theoretical mass obtained in each channel is shown in the second column, and the binding energy is presented in the following one. A mixture of color-singlet and -octet states for each baryon–meson configuration is considered, and the coupled mass and binding energy are shown in the last column. The lowest-lying mass in a partially coupled-channel calculation, which includes the color-singlet and -octet channel coupling, and a complete coupled-channel one is performed, and they are indicated at the bottom of the table, respectively (unit: MeV).

| Channel	M	E_B	Mixed $(M_{1 \oplus 8}, E_B)$
$(\Lambda \eta_c)^1$ (4097)	3918	0	(3918, 0)
$(\Lambda \eta_c)^8$	4782	+864	
$(\Lambda_c D_s)^1$ (4255)	4029	0	(4029, 0)
$(\Lambda_c D_s)^8$	4730	+701	
$(\Xi'_c D)^1$ (4448)	4509	−5	(4058, −6)
$(\Xi'_c D)^8$	4818	+304	
$(\Xi_c D)^1$ (4340)	4289	−11	(4289, −11)
$(\Xi_c D)^8$	4762	+462	
$(\Lambda J/\psi)^1$ (4213)	4025	0	(4025, 0)
$(\Lambda J/\psi)^8$	4759	+734	
$(\Lambda_c D_s^*)^1$ (4399)	4165	0	(4165, 0)
$(\Lambda_c D_s^*)^8$	4677	+512	
$(\Xi'_c D^*)^1$ (4585)	4627	−4	(4614, −17)
$(\Xi'_c D^*)^8$	4783	+152	
$(\Xi_c D^*)^1$ (4477)	4410	−7	(4408, −9)
$(\Xi_c D^*)^8$	4686	+269	
$(\Xi_c^* D^*)^1$ (4652)	4671	−5	(4617, −59)
$(\Xi_c^* D^*)^8$	4657	−19	
All color-singlet channels coupling:			3918
All color-octet channels coupling:			4653
Complete coupled-channel:			3918
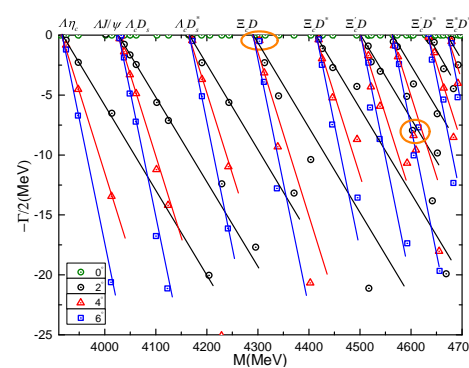
Figure 3. Complex energies of complete coupled-channel calculation for the $qqsc\bar{c}$ pentaquark within $IJ^P = 0(\frac{1}{2}^-)$.

Table 5. The compositeness of exotic resonances obtained in a complete coupled-channel computation in the $0(\frac{1}{2}^-)$ state of the $qqsc\bar{c}$ pentaquark. Particularly, the first column is the resonance pole labeled by $M + i\Gamma$, with unit MeV; the second one is the distance between any two quarks ($q = u, d, s$) or quark–antiquark, with unit fm, and the dominant component of the resonance state (S: baryon–meson structure in a color-singlet channel; H: baryon–meson structure in a hidden-color channel).

Resonance	Structure
$4303 + i1.0$	$r_{qq} : 0.99$; $\ r_{qc} : 1.50$; $\ r_{q\bar{c}} : 1.59$; $\ r_{c\bar{c}} : 0.97$
	S: 90.7%; $\ $ H: 9.3%
	$(\Lambda J/\psi)$ [1]: 60%; $\ (\Xi_c D)$ [1]: 23%
$4603 + i15.9$	$r_{qq} : 1.06$; $\ r_{qc} : 1.80$; $\ r_{q\bar{c}} : 1.88$; $\ r_{c\bar{c}} : 1.16$
	S: 89%; $\ $ H: 11%
	$(\Lambda \eta_c)$ [1]: 21%; $\ (\Lambda J/\psi)$ [1]: 29%; $\ (\Lambda_c D_s)$ [1]: 13%

The $I(J^P) = 0(\frac{1}{2}^-)$ channel: All of the possible baryon–meson channels, $\Lambda\eta_c$, $\Lambda J/\psi$, $\Lambda_c D_s^{(*)}$, $\Xi_c' D^{(*)}$ and $\Xi_c^{(*)} D^{(*)}$, listed in Table 4, are firstly investigated in a real-range calculation. The lowest channel, $\Lambda\eta_c$, has a theoretical mass of 3918 MeV, which is just the theoretical threshold value, and it is a scattering state. The unbound nature also holds for other $(qqs)(c\bar{c})$ and $(qqc)(s\bar{c})$ configurations, viz., the color-singlet channels of $\Lambda J/\psi$ and $\Lambda_c D_s^{(*)}$ configurations are all of scattering type. In addition, the coupling effect is quite weak in these cases when considering their respective hidden-color channels; hence, the scattering nature remains. On the other hand, bound states are found in the $(qsc)(q\bar{c})$ configuration; particularly, five baryon–meson channels contribute, i.e., $\Xi_c' D$, $\Xi_c D$, $\Xi_c' D^*$, $\Xi_c D^*$ and $\Xi_c^* D^*$. There are binding energies which range from -4 to -11 MeV for the color-singlet channels. Concerning the $\Xi_c D$ channel, which has -11 MeV binding energy and then 4.33 GeV attending to its experimental threshold, it is quite compatible with the reported $P_{cs}(4338)$ state [4]. However, the stability of this state needs to be confirmed in a further coupled-channel analysis. Meanwhile, hidden-color channels of these kinds of configurations predict unbounded states, except for a -19 MeV binding energy of the color-octet $\Xi_c^* D^*$. This color resonance becomes more tightly bound with $M = 4617$ MeV and $E_B = -59$ MeV if the singlet and octet channels are all coupled, while the coupling is weak in other $\Xi_c^{(*)} D^{(*)}$ channels.

In a further step, three types of coupled-channel computations, all color-singlets, all color-octets and fully coupled, are performed with $\theta = 0°$ (real-range calculation). The lowest-lying masses are listed at the bottom of Table 4. Particularly, the scattering nature of the lowest channel, $\Lambda\eta_c$, remains in this kind of computation; moreover, a color-octet resonant signal at 4653 MeV is also obtained.

In order to better understand the spectrum of $qqsc\bar{c}$ pentaquarks with quantum numbers $I(J^P) = 0(\frac{1}{2}^-)$, the CSM is adopted by considering a rotated angle ranging from $2°$ to $6°$. The distribution of calculated complex energies is plotted in Figure 3. Therein, with an energy interval from 3.9 to 4.7 GeV, the nine scattering states of $\Lambda\eta_c$, $\Lambda J/\psi$, $\Lambda_c D_s^{(*)}$, $\Xi_c' D^{(*)}$ and $\Xi_c^{(*)} D^{(*)}$ are well presented. The vast majority of energy dots are aligned along the corresponding threshold lines; however, two stable poles are obtained and they are circled.

Table 5 collects information about the two resonances obtained in a complete coupled-channel computation by the CSM. Firstly, their masses and widths (M, Γ) are $(4303, 1.0)$ MeV and $(4603, 15.9)$ MeV, respectively. Apparently, the lower resonance can be identified as the $P_{cs}(4338)$ state. The dominant two-body strong decay widths are the color-singlet channels $\Lambda J/\psi(60\%)$ and $\Xi_c D(23\%)$. Its size is less than 1.6 fm. Moreover, the higher resonance at 4.6 GeV has a width of 15.9 MeV, which is mainly given by the final states of $\Lambda\eta_c(21\%)$, $\Lambda J/\psi(29\%)$ and $\Lambda_c D_s(13\%)$ in the singlet color channel. This exotic state, whose size is less than 1.9 fm, is expected to be confirmed in future experiments.

Table 6. The lowest-lying $qqsc\bar{c}$ pentaquark states with $I(J^P) = 0(\frac{3}{2}^-)$ calculated in a real-range formulation of the potential model. This table is similarly organized as Table 4 (unit: MeV).

| Channel	M	E_B	Mixed $(M_{\mathbf{1 \oplus 8}}, E_B)$
$(\Lambda J/\psi)^1$ (4213)	4025	0	$(4025, 0)$
$(\Lambda J/\psi)^8$	4793	$+768$	
$(\Lambda_c D_s^*)^1$ (4399)	4166	0	$(4166, 0)$
$(\Lambda_c D_s^*)^8$	4746	$+580$	
$(\Xi_c' D^*)^1$ (4585)	4628	-3	$(4628, -3)$
$(\Xi_c' D^*)^8$	4898	$+267$	
$(\Xi_c D^*)^1$ (4477)	4411	-7	$(4411, -7)$
$(\Xi_c D^*)^8$	4787	$+369$	
$(\Xi_c^* D)^1$ (4515)	4555	-4	$(4553, -6)$
$(\Xi_c^* D)^8$	4853	$+294$	
$(\Xi_c^* D^*)^1$ (4652)	4674	-2	$(4656, -20)$
$(\Xi_c^* D^*)^8$	4771	$+95$	
All color-singlet channels coupling:			4025
All color-octet channels coupling:			4725
Complete coupled-channel:			4025
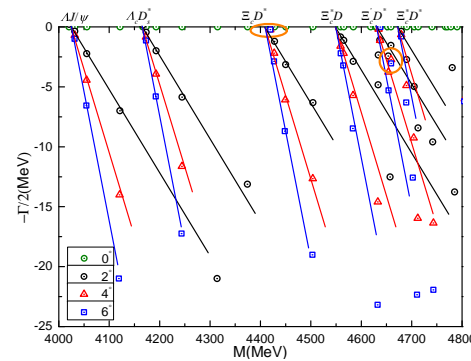
Figure 4. The complex energies of complete coupled-channel calculation for the $qqsc\bar{c}$ pentaquark within $IJ^P = 0(\frac{3}{2}^-)$.

Table 7. Compositeness of exotic resonances obtained in complete coupled-channel computation in $0(\frac{3}{2}^-)$ state of $qqsc\bar{c}$ pentaquark. Results are similarly organized as those in Table 5.

Resonance	Structure
$4419 + i0.5$	$r_{qq}: 1.80;\quad r_{qc}: 1.32;\quad r_{q\bar{c}}: 1.75;\quad r_{c\bar{c}}: 2.03$
	S: 89.6%; H: 10.4%
	$(\Xi_c D^*)^1$: 72%
$4659 + i5.4$	$r_{qq}: 1.70;\quad r_{qc}: 2.15;\quad r_{q\bar{c}}: 2.40;\quad r_{c\bar{c}}: 1.94$
	S: 93.8%; H: 6.2%
	$(\Lambda J/\psi)^1$: 28%; $(\Xi_c' D^*)^1$: 19%
	$(\Xi_c D^*)^1$: 19%; $(\Xi_c^* D)^1$: 13%

The $I(J^P) = 0(\frac{3}{2}^-)$ channel: Table 6 lists our results of hidden-charm pentaquarks with strangeness in the mentioned channel obtained by the real-range calculation. In particular, $\Lambda J/\psi$, $\Lambda_c D_s^*$, $\Xi_c' D^*$ and $\Xi_c^{(*)} D^{(*)}$ are all the configurations considered. First, the lowest mass 4025 MeV is the theoretical threshold value of $\Lambda J/\psi$; hence, it is just a scattering state. In addition, the second energy level, which lies at 4166 MeV, is the theoretical threshold of $\Lambda_c D_s^*$, and the unbound nature is also concluded. The scattering feature of the $(qqs)(c\bar{c})$

and $(qqc)(s\bar{c})$ configurations is characteristic of the coupled-channel studies that consider either singlet- or color-octet channels. Particularly, the excited energy values of $(\Lambda J/\psi)^8$ and $(\Lambda_c D_s^*)^8$ are 768 and 580 MeV, respectively. However, as in the channel $I(J^P) = 0(\frac{1}{2}^-)$, bound states are found in the $(qsc)(q\bar{c})$ configuration. From Table 6, one can find ~ 4 MeV binding energies for color-singlet channels $\Xi_c' D^*$, $\Xi_c D^*$, $\Xi_c^* D$ and $\Xi_c^* D^*$. Their hidden-color or color-octet channels are generally 300 MeV higher than theoretical thresholds, except for the $(\Xi_c^* D^*)^8$ state with 95 MeV exciting energy. Additionally, after a mixture of the singlet- and hidden-color channels, the lowest mass values of $\Xi_c^* D$ and $\Xi_c^* D^*$ shift to 4553 and 4656 MeV, respectively. However, $\Xi_c' D^*$ and $\Xi_c D^*$ remain at 4268 and 4411 MeV, respectively. Herein, the $\Xi_c D^*$ bound state, which has a binding energy of -7 MeV and a modified mass of 4470 MeV, is compatible with $P_{cs}(4459)$ in the $I(J^P) = 0(\frac{3}{2}^-)$ state [3].

At the bottom of Table 6, we show the lowest coupled mass in three types of real-range calculations. When all color-singlet channels are considered, the lowest mass, 4025 MeV, is still the theoretical threshold value of the $\Lambda J/\psi$ channel. This weak coupling effect remains in the complete coupled-channel calculation. In addition, a color resonance of 4725 MeV is obtained in a computation with all hidden-color channels included.

The spectrum of $qqsc\bar{c}$ pentaquarks with isospin and spin-parity $0(\frac{3}{2}^-)$ is now investigated in a fully coupled calculation with the help of the CSM; see Figure 4. Within an energy range of $4.0 - 4.8$ GeV, the scattering states of $\Lambda J/\psi$, $\Lambda_c D_s^*$, $\Xi_c D^*$, $\Xi_c^* D$, $\Xi_c' D^*$ and $\Xi_c^* D^*$ are clearly shown. However, two stable poles are obtained and circled. Their complex energies read as $4419 + i0.5$ MeV and $4659 + i5.4$ MeV, respectively. Moreover, quark–(anti-)quark distances and the dominant components of resonances are listed in Table 7. The first resonance at 4.42 GeV is quite compatible with the $P_{cs}(4459)$ state [3]. Its size is less than 2.0 fm, and the golden channel is $\Xi_c D^*(72\%)$ in our calculation. In addition, since the calculated distance between q and $\bar{c}$ is 2.4 fm, a loosely resonant nature of the second state at 4.66 GeV can be drawn. There is a strong coupling among the color-singlet channels $\Lambda J/\psi(28\%)$, $\Xi_c' D^*(19\%)$, $\Xi_c D^*(19\%)$ and $\Xi_c^* D(13\%)$. Accordingly, the narrow resonance, $4659 + i5.4$ MeV, is also expected to be found in future high-energy experimental facilities.

Table 8. The lowest-lying $qqsc\bar{c}$ pentaquark states with $I(J^P) = 0(\frac{5}{2}^-)$ calculated in a real-range formulation of the potential model. This table is similarly organized as Table 4 (unit: MeV).

| Channel	M	E_B	Mixed $(M_{1\oplus 8}, E_B)$
$(\Xi_c^* D^*)^1$ (4652)	4673	-3	(4673, -3)
$(\Xi_c^* D^*)^8$	5003	$+327$	
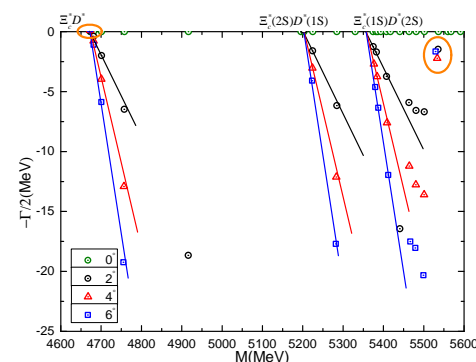
Figure 5. Complex energies of complete coupled-channel calculation for $qqsc\bar{c}$ pentaquark within $IJ^P = 0(\frac{5}{2}^-)$.

Table 9. Compositeness of exotic states obtained in complete coupled-channel computation in $0(\frac{5}{2}^{-})$ state of $qqsc\bar{c}$ pentaquark. Results are similarly organized as those in Table 5.

Exotic State	Structure
$4673 + i0$	r_{qq} : 1.86; r_{qc} : 1.36; $r_{q\bar{c}}$: 1.78; $r_{c\bar{c}}$: 2.05
$(E_B = -3)$	$(\Xi_c^* D^*)$ [1]: 97.4%; $(\Xi_c^* D^*)$ [8]: 2.6%
$5533 + i3.4$	r_{qq} : 1.55; r_{qc} : 1.18; $r_{q\bar{c}}$: 1.28; $r_{c\bar{c}}$: 0.89
	$(\Xi_c^* D^*)$ [1]: 49.5%; $(\Xi_c^* D^*)$ [8]: 50.5%

The $I(J^P) = 0(\frac{5}{2}^{-})$ channel: Only one baryon–meson channel, $\Xi^* D^*$, contributes to the highest spin channel within the isoscalar sector. Firstly, in the single-channel calculation that includes the color-singlet and -octet configurations, the lowest-lying mass values are 4673 and 5003 MeV, respectively, which correspond to binding energy values of -3 and 327 MeV, when compared to the theoretical threshold. Moreover, the channel-coupling effect is extremely weak in this case, and thus the coupled mass remains at 4673 MeV.

A complex-range analysis of fully coupled-channel calculation is then performed, and results are presented in Figure 5. In the 4.6–5.6 GeV energy region, three scattering states, which include $\Xi^*(1S)D^*(1S)$ and its radial excited cases $\Xi^*(2S)D^*(1S)$ and $\Xi^*(1S)D^*(2S)$, are well presented. Moreover, one bound state and one narrow resonance are also obtained. Firstly, the mentioned $\Xi^* D^*$ again appears loosely bound. Secondly, a narrow resonance with $\Gamma = 3.4$ MeV is obtained at 5533 MeV. It is compact, with size around 1.2 fm, and there is a strong coupling between the color-singlet (50%) and -octet (50%) channels of $\Xi^* D^*$.

Table 10. The lowest-lying $qqsc\bar{c}$ pentaquark states with $I(J^P) = 1(\frac{1}{2}^{-})$ calculated in a real-range formulation of the potential model. This table is similarly organized as Table 4 (unit: MeV).

| Channel	M	E_B	Mixed $(M_{1 \oplus 8}, E_B)$
$(\Sigma \eta_c)$ [1] (4174)	4084	0	(4084, 0)
$(\Sigma \eta_c)$ [8]	4837	+753	
$(\Sigma J/\psi)$ [1] (4290)	4192	0	(4192, 0)
$(\Sigma J/\psi)$ [8]	4818	+626	
$(\Sigma^* J/\psi)$ [1] (4482)	4477	0	(4477, 0)
$(\Sigma^* J/\psi)$ [8]	4807	+330	
$(\Sigma_c D_s)$ [1] (4422)	4501	0	(4501, 0)
$(\Sigma_c D_s)$ [8]	4906	+405	
$(\Sigma_c D_s^*)$ [1] (4566)	4636	0	(4636, 0)
$(\Sigma_c D_s^*)$ [8]	4877	+241	
$(\Sigma_c^* D_s^*)$ [1] (4632)	4679	0	(4621, -58)
$(\Sigma_c^* D_s^*)$ [8]	4645	-34	
$(\Xi_c' D)$ [1] (4448)	4514	0	(4514, 0)
$(\Xi_c' D)$ [8]	4909	+395	
$(\Xi_c D)$ [1] (4340)	4301	0	(4301, 0)
$(\Xi_c D)$ [8]	4752	+451	
$(\Xi_c' D^*)$ [1] (4585)	4631	0	(4631, 0)
$(\Xi_c' D^*)$ [8]	4908	+277	
$(\Xi_c D^*)$ [1] (4477)	4418	0	(4418, 0)
$(\Xi_c D^*)$ [8]	4695	+277	
$(\Xi_c^* D^*)$ [1] (4652)	4676	0	(4676, 0)
$(\Xi_c^* D^*)$ [8]	4857	+181	
All color-singlet channels coupling:			4084
All color-octet channels coupling:			4563
Complete coupled-channel:			4084
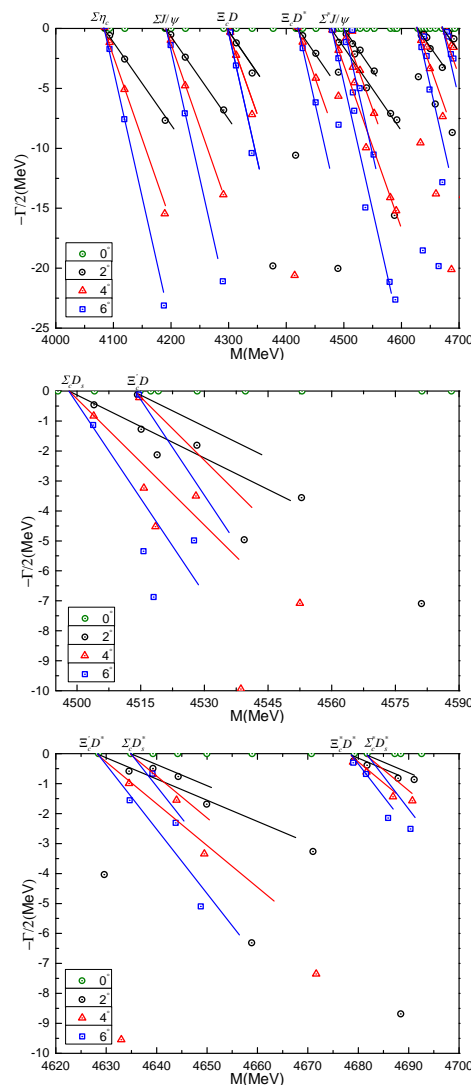
Figure 6. (**Top panel**): The complex energies of complete coupled-channel calculation for the $qqsc\bar{c}$ pentaquark within $IJ^P = 1(\frac{1}{2}^-)$. (**Middle panel**): Enlarged top panel, with real values of energy ranging from 4.49 GeV to 4.59 GeV. (**Bottom panel**): Enlarged top panel, with real values of energy ranging from 4.62 GeV to 4.70 GeV.

The $I(J^P) = 1(\frac{1}{2}^-)$ channel: Table 10 lists the real-range calculations of the $qqsc\bar{c}$ pentaquarks with isovector character and spin-parity $\frac{1}{2}^-$. We consider 11 baryon–meson configurations, and they are $\Sigma\eta_c$, $\Sigma^{(*)}J/\psi$, $\Sigma_c^{(*)}D_s^{(*)}$, $\Xi_c'D^{(*)}$ and $\Xi_c^{(*)}D^{(*)}$. Firstly, the lowest-lying state in the color-singlet channels is $\Sigma\eta_c$ with calculated mass 4084 MeV. Since its mass is located just at the theoretical threshold value, a scattering nature is deduced, and this unbound feature also holds for other singlet color channels. However, one bound state with mass and binding energy 4645 and -34 MeV, respectively, is found in the hidden-color channel of the $\Sigma_c^*D_s^*$ state. When a color–structure mixture is considered, this bound state is pushed down towards 4621 MeV, with a deeper binding energy of -58 MeV. Other hidden-color channels are generally $200 - 750$ MeV higher than their corresponding thresholds, and the coupled-channels mechanism of color structures does not help in forming a bound state.

Furthermore, as shown at the bottom of Table 10, in the three types of coupled-channel calculations, the scattering nature of the $\Sigma\eta_c$ state remains unchanged, while a color resonance at 4563 MeV is obtained by only considering hidden-color channels' coupling.

The stability of the bound and color resonance states at 4621 and 4563 MeV, respectively, should be further studied in a complete coupled-channel calculation by using the CSM. Figure 6 shows the distribution of complex energies. Particularly, the scattering states of $\Sigma\eta_c$, $\Sigma J/\psi$, $\Xi_c D$, $\Xi_c D^*$ and $\Sigma^* J/\psi$ are presented in the top panel, and no stable pole is found within 4.0–4.5 GeV. An enlarged part from 4.49–4.59 GeV is plotted in the middle panel of Figure 6. Therein, the resonance pole is still unavailable, and the scattering states of $\Sigma_c D_s$ and $\Xi_c' D$ are presented. Hence, the previous color resonance at 4563 MeV did not survive in a fully coupled-channel case. Finally, in the bottom panel, whose energy range goes from 4.62 to 4.70 GeV, four scattering states corresponding to $\Xi' D^*$, $\Sigma_c D_s^*$, $\Xi_c^* D^*$ and $\Sigma_c^* D_s^*$ are shown, and there is no evidence of a resonance state. Accordingly, the $(\Sigma_c^* D^*)^8$ bound state, which was obtained in a partial channel coupling computation, is quite unstable.

Table 11. The lowest-lying $qqsc\bar{c}$ pentaquark states with $I(J^P) = 1(\frac{3}{2}^-)$ calculated in a real-range formulation of the potential model. This table is similarly organized as Table 4 (unit: MeV).

Channel	M	E_B	Mixed $(M_{1\oplus 8}, E_B)$
$(\Sigma J/\psi)^1$ (4290)	4192	0	(4192, 0)
$(\Sigma J/\psi)^8$	4845	+653	
$(\Sigma^*\eta_c)^1$ (4366)	4370	0	(4370, 0)
$(\Sigma^*\eta_c)^8$	4857	+487	
$(\Sigma^* J/\psi)^1$ (4482)	4477	0	(4477, 0)
$(\Sigma^* J/\psi)^8$	4837	+360	
$(\Sigma_c D_s^*)^1$ (4566)	4636	0	(4636, 0)
$(\Sigma_c D_s^*)^8$	4912	+276	
$(\Sigma_c^* D_s)^1$ (4488)	4543	0	(4543, 0)
$(\Sigma_c^* D_s)^8$	4735	+192	
$(\Sigma_c^* D_s^*)^1$ (4632)	4679	0	(4669, −10)
$(\Sigma_c^* D_s^*)^8$	4698	+19	
$(\Xi_c' D^*)^1$ (4585)	4631	0	(4631, 0)
$(\Xi_c' D^*)^8$	4888	+257	
$(\Xi_c D^*)^1$ (4477)	4418	0	(4418, 0)
$(\Xi_c D^*)^8$	4772	+354	
$(\Xi_c^* D)^1$ (4515)	4559	0	(4676, 0)
$(\Xi_c^* D)^8$	4856	+297	
$(\Xi_c^* D^*)^1$ (4652)	4676	0	(4676, 0)
$(\Xi_c^* D^*)^8$	4848	+172	
All color-singlet channels coupling:			4192
All color-octet channels coupling:			4524
Complete coupled-channel:			4192
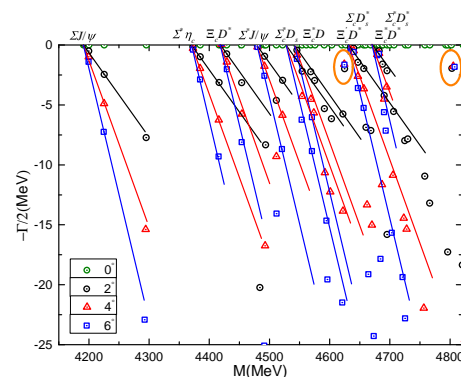
Figure 7. Complex energies of complete coupled-channel calculation for $qqsc\bar{c}$ pentaquark within $IJ^P = 1(\frac{3}{2}^-)$.

Table 12. Compositeness of exotic resonances obtained in complete coupled-channel computation in $1(\frac{3}{2}^-)$ state of $qqsc\bar{c}$ pentaquark. Results are similarly organized as those in Table 5.

Resonance	Structure
$4625 + i4.0$	$r_{qq} : 1.60$; $r_{qc} : 1.19$; $r_{q\bar{c}} : 1.53$; $r_{c\bar{c}} : 1.72$
	S: 87%; H: 13%
	$(\Sigma_c D_s^*)\,^1$: 33%; $(\Sigma_c^* D_s)\,^1$: 12%; $(\Xi_c' D^*)\,^1$: 21%
$4803 + i3.9$	$r_{qq} : 1.39$; $r_{qc} : 1.60$; $r_{q\bar{c}} : 1.77$; $r_{c\bar{c}} : 1.40$
	S: 90.6%; H: 9.4%
	$(\Sigma^* J/\psi)\,^1$: 27%; $(\Xi_c^* D)\,^1$: 21%; $(\Xi_c^* D^*)\,^1$: 14%

The $I(J^P) = 1(\frac{3}{2}^-)$ channel: A total of 10 baryon–meson configurations listed in Table 11 are investigated herein. Among the $\Sigma^{(*)} J/\psi$, $\Sigma^* \eta_c$, $\Sigma_c^{(*)} D_s^{(*)}$, $\Xi_c' D^*$ and $\Xi_c^{(*)} D^{(*)}$ channels both in color-singlet and hidden-color arrangements, the lowest-lying one is $\Sigma J/\psi$, and its mass is 4192 MeV, which is just the theoretical value of the non-interacting baryon–meson threshold. Moreover, bound states are still not obtained in other channel calculations, and hidden-color channels are generally excited by an energy of 200–650 MeV, except the color-octet channel of $\Sigma_c^* D_s^*$, which is 19 MeV higher than its theoretical threshold. Furthermore, a weakly bound state, whose mass and binding energy are 4669 and -10 MeV, respectively, is obtained in the $\Sigma_c^* D_s^*$ configuration when the singlet- and hidden-color channels are mixed.

When we perform a coupled-channel calculation within the real-range formalism, taking into account all singlet channels, all octet channels and a fully coupled case, bound states are not obtained, the lowest-lying mass, 4192 MeV, is the $\Sigma J/\psi$ theoretical threshold value, and a color-octet resonance located at 4524 MeV is found.

Figure 7 shows the distribution of complex energies in a fully coupled-channel study using the CSM. Within the mass interval of $4.15 - 4.85$ GeV, the scattering states of $\Sigma^{(*)} J/\psi$, $\Sigma^* \eta_c$, $\Sigma_c^{(*)} D_s^{(*)}$, $\Xi_c' D^*$ and $\Xi_c^{(*)} D^{(*)}$ are clearly found. Apart from them, two stable poles are circled in the complex energy plane. Their nature and structural information can be found in Table 12. In particular, the lower resonance is at 4625 MeV, and the higher one is at 4803 MeV. Their two-body strong decay widths are 4 MeV. In addition, they have similar sizes, which are about 1.5 fm. Color-singlet channels account for the dominant contributions to their wave functions: $\Sigma_c D_s^*(33\%)$, $\Sigma_c^* D_s(12\%)$ and $\Xi_c' D^*(21\%)$ for the lower resonance, whereas $\Sigma^* J/\psi(27\%)$, $\Xi_c^* D(21\%)$ and $\Xi_c^* D^*(14\%)$ are for the other one.

Table 13. The lowest-lying $qqsc\bar{c}$ pentaquark states with $I(J^P) = 1(\frac{5}{2}^-)$ calculated in a real-range formulation of the potential model. This table is similarly organized as Table 4 (unit: MeV).

| Channel	M	E_B	Mixed $(M_{1\oplus 8}, E_B)$
$(\Sigma^* J/\psi)\,^1$ (4482)	4477	0	(4477, 0)
$(\Sigma^* J/\psi)\,^8$	4883	+406	
$(\Sigma_c^* D_s^*)\,^1$ (4632)	4679	0	(4679, 0)
$(\Sigma_c^* D_s^*)\,^8$	4773	+94	
$(\Xi_c^* D^*)\,^1$ (4652)	4676	0	(4676, 0)
$(\Xi_c^* D^*)\,^8$	4853	+177	
All color-singlet channels coupling:			4477
All color-octet channels coupling:			4700
Complete coupled-channel:			4477
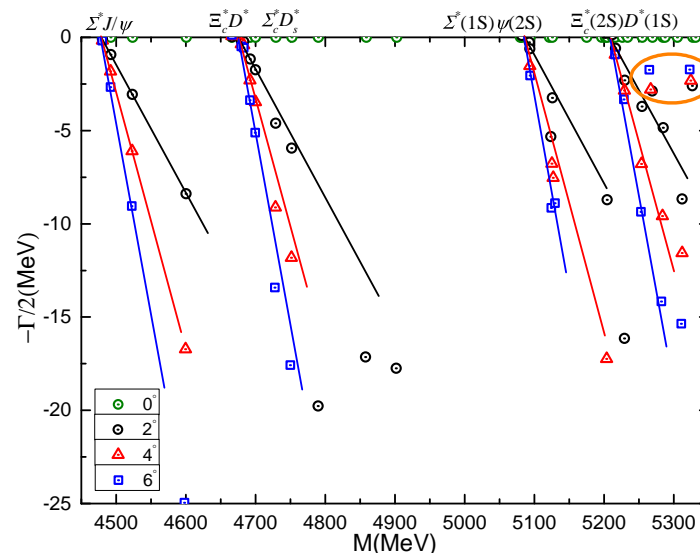
Figure 8. Complex energies of complete coupled-channel calculation for $qqsc\bar{c}$ pentaquark within $IJ^P = 1(\frac{5}{2}^{-})$.

Table 14. Compositeness of exotic states obtained in a complete coupled-channel computation in $1(\frac{5}{2}^{-})$ state of $qqsc\bar{c}$ pentaquark. Results are similarly organized as those in Table 5.

Resonance	Structure
$5269 + i5.8$	$r_{qq}: 1.39$; $r_{qc}: 1.29$; $r_{q\bar{c}}: 1.38$; $r_{c\bar{c}}: 1.11$
	$S: 54\%$; $H: 46\%$ $(\Sigma^* J/\psi)^{1}: 43\%$; $(\Sigma_c^* D_s^*)^{8}: 29.4\%$
$5327 + i5.2$	$r_{qq}: 1.38$; $r_{qc}: 1.19$; $r_{q\bar{c}}: 1.28$; $r_{c\bar{c}}: 1.11$
	$S: 54.3\%$; $H: 45.7\%$ $(\Sigma^* J/\psi)^{1}: 36.2\%$; $(\Sigma_c^* D_s^*)^{8}: 34.1\%$

$I(J^P) = 1(\frac{5}{2}^{-})$ **channel:** Three baryon–meson configurations should be considered in the highest spin case of the isovector sector, and they are indicated in Table 13. Particularly, the lowest-lying state is $\Sigma^* J/\psi$ with a theoretical mass of 4477 MeV; the two others lie at 4679 and 4676 MeV for $\Sigma_c^* D_s^*$ and $\Xi_c^* D^*$, respectively. Hidden-color channels are at least 90 MeV higher in energy than theoretical threshold lines. Accordingly, no bound states are found, and this result is also obtained within coupled-channel calculations; see the bottom part of Table 13. However, a color resonance located at 4.7 GeV is obtained within a coupled-channel analysis in which only hidden-color configurations are included.

Additionally, when a complex-range investigation is performed, considering all of the $1\frac{5}{2}^{-}$ channels, two narrow resonances are found. Figure 8 shows the scattering states corresponding to $\Sigma^* J/\psi$, $\Sigma_c^* D_s^*$ and $\Xi_c^* D^*$ within an energy region of 4.45–5.35 GeV. Moreover, two stable poles are circled, and their complex energies read $5269 + i5.8$ and $5327 + i5.2$ MeV, respectively. By looking at Table 14, which provides structural information for the two singularities, a strong coupling effect between the color-singlet ($\sim 54\%$) and -octet ($\sim 46\%$) channels is found in both cases. Moreover, the dominant components are also the same: $(\Sigma^* J/\psi)^{1}$ and $(\Sigma_c^* D_s^*)^{8}$. Additionally, one can also find similarities between the two resonances when looking at their inner quark distances. Generally, their sizes are around 1.3 fm.

Table 15. A summary of exotic structures found in the $qqsc\bar{c}$ ($q = u, d$) pentaquark systems. The first column shows the isospin, total spin and parity of each singularity. If available, the second column lists well-known experimental states, which may be identified in our theoretical framework. The third column refers to the dominant configuration components, particularly, the superscripts 1 and 8 stand for color-singlet and -octet states, respectively. For a concise purpose, the component without superscripts is of singlet color state. Theoretical bound and resonance states are presented with the following notation: (M, E_B) and $M + i\Gamma$ in the last column, respectively (unit: MeV).

$I(J^P)$	Experimental State	Dominant Component	Theoretical Pole
$0(\frac{1}{2}^-)$	$P_{cs}(4338)$	$\Lambda J/\psi(60\%) + \Xi_c D(23\%)$	$4303 + i1.0$
		$\Lambda\eta_c(21\%) + \Lambda J/\psi(29\%) + \Lambda_c D_s(13\%)$	$4603 + i15.9$
$0(\frac{3}{2}^-)$	$P_{cs}(4459)$	$\Xi_c D^*(72\%)$	$4419 + i0.5$
		$\Lambda J/\psi(28\%) + \Xi_c^{(')} D^*(19\%) + \Xi_c^* D(13\%)$	$4659 + i5.4$
$0(\frac{5}{2}^-)$		$\Xi_c^* D^*(97.4\%)$	$(4673, -3)$
		$(\Xi_c^* D^*)^1(49.5\%) + (\Xi_c^* D^*)^8(50.5\%)$	$5533 + i3.4$
$1(\frac{3}{2}^-)$		$\Sigma_c D_s^*(33\%) + \Sigma_c^* D_s(12\%) + \Xi_c' D^*(21\%)$	$4625 + i4.0$
		$\Sigma^* J/\psi(27\%) + \Xi_c^* D(21\%) + \Xi_c^* D^*(14\%)$	$4803 + i3.9$
$1(\frac{5}{2}^-)$		$(\Sigma^* J/\psi)^1(43\%) + (\Sigma_c^* D_s^*)^8(29.4\%)$	$5269 + i5.8$
		$(\Sigma^* J/\psi)^1(36.2\%) + (\Sigma_c^* D_s^*)^8(34.1\%)$	$5327 + i5.2$

4. Summary

S-wave hidden-charm pentaquarks with strangeness, $qqsc\bar{c}$ ($q = u, d$), whose spin-parities are $J^P = \frac{1}{2}^-$, $\frac{3}{2}^-$ and $\frac{5}{2}^-$ and isospins either 0 or 1, have been systematically investigated within a chiral quark model approach that employs a highly accurate computational method, the Gaussian expansion formalism (GEM), along with the complex scaling technique (CSM), which is a powerful tool when dealing simultaneously with bound, resonant and scattering states.

Within this theoretical framework, and by considering baryon–meson configurations in both singlet- and hidden-color channels, the two experimentally reported P_{cs} states [3,4] can be well identified. In addition, other structures can be distinguished in the different channels, except for the $I(J^P) = 1(\frac{1}{2}^-)$ one. Table 15 summarizes our theoretical findings on $qqsc\bar{c}$ pentaquarks. In particular, the $I(J^P)$ quantum numbers are indicated in the first column, plausible experimental assignments are listed in the following one, the third column shows the dominant components in the wave functions of exotic states, and their theoretical pole positions are presented in the last column.

The following details of our analysis are of particular interest. Firstly, the experimentally reported $P_{cs}(4338)$ and $P_{cs}(4459)$ signals, whose tentative assignments of spin-parity are $\frac{1}{2}^-$ and $\frac{3}{2}^-$, respectively, can be well identified within our theoretical framework as molecules in the isoscalar sector. The dominant components of the lower-energy state are $\Lambda J/\psi$ (60%) and $\Xi_c D$ (23%), while it is the $\Xi_c D^*$ (72%) structure that is dominant in the higher-energy candidate. Secondly, narrow resonances are obtained in all of the allowed $I(J^P)$ channels, except for the $1(\frac{1}{2}^-)$ one. Generally, they are located in a mass region from 4.6 to 5.5 GeV, and they have strong couplings to different color-singlet channels. In the $J^P = \frac{5}{2}^-$ channels, both isoscalar and isovector, the color-singlet and -octet configurations couple strongly. Finally, a $\Xi_c^* D^*$ shallow bound state is obtained in the $0(\frac{5}{2}^-)$ channel. The theoretical mass and binding energy are 4673 MeV and -3 MeV, respectively.

All of the above findings are expected to be confirmed in future high-energy experiments.

References

1. The LHCb Collaboration. Observation of $J/\psi p$ Resonances Consistent with Pentaquark States in $\Lambda_b^0 \to J/\psi K^- p$ Decays. *Phys. Rev. Lett.* **2015**, *115*, 072001. [CrossRef]
2. The LHCb Collaboration. Observation of a narrow pentaquark state, $P_c(4312)^+$, and of two-peak structure of the $P_c(4450)^+$. *Phys. Rev. Lett.* **2019**, 122, 222001. [CrossRef]
3. The LHCb Collaboration. Evidence of a $J/\psi\Lambda$ structure and observation of excited Ξ^- states in the $\Xi_b^- \to J/\psi\Lambda K^-$ decay. *Sci. Bull.* **2021**, *66*, 1278–1287. [CrossRef]
4. The LHCb Collaboration. Observation of a J/$\psi\Lambda$ Resonance Consistent with a Strange Pentaquark Candidate in B-$\to$J/$\psi\Lambda$p$^-$ Decays. *Phys. Rev. Lett.* **2023**, *131*, 031901. [CrossRef] [PubMed]
5. Feijoo, A.; Wang, W.F.; Xiao, C.W.; Wu, J.J.; Oset, E.; Nieves, J.; Zou, B.S. A new look at the Pcs states from a molecular perspective. *Phys. Lett. B* **2023**, *839*, 137760. [CrossRef]
6. Zhu, J.T.; Kong, S.Y.; He, J. PψsΛ(4459) and PψsΛ(4338) as molecular states in J/$\psi\Lambda$ invariant mass spectra. *Phys. Rev. D* **2023**, *107*, 034029. [CrossRef]
7. Yan, M.J.; Peng, F.Z.; Sánchez Sánchez, M.; Pavon Valderrama, M. PψsΛ(4338) pentaquark and its partners in the molecular picture. *Phys. Rev. D* **2023**, *107*, 074025. [CrossRef]
8. Chen, R.; Liu, X. Mass behavior of hidden-charm open-strange pentaquarks inspired by the established P_c molecular states. *Phys. Rev. D* **2022**, *105*, 014029. [CrossRef]
9. Du, M.L.; Guo, Z.H.; Oller, J.A. Insights into the nature of the Pcs(4459). *Phys. Rev. D* **2021**, *104*, 114034. [CrossRef]
10. Zhu, J.T.; Song, L.Q.; He, J. $P_{cs}(4459)$ and other possible molecular states from $\Xi_c^{(*)}\bar{D}^{(*)}$ and $\Xi_c'\bar{D}^{(*)}$ interactions. *Phys. Rev. D* **2021**, *103*, 074007. [CrossRef]
11. Wang, X.W.; Wang, Z.G. Analysis of P $_{cs}$(4338) and related pentaquark molecular states via QCD sum rules*. *Chin. Phys. C* **2023**, *47*, 013109. [CrossRef]
12. Wang, X.W.; Wang, Z.G. Study of isospin eigenstates of the pentaquark molecular states with strangeness. *Int. J. Mod. Phys. A* **2022**, *37*, 2250189. [CrossRef]
13. Wang, Z.G. Analysis of the $P_{cs}(4459)$ as the hidden-charm pentaquark state with QCD sum rules. *Int. J. Mod. Phys. A* **2021**, *36*, 2150071. [CrossRef]
14. Chen, H.X.; Chen, W.; Liu, X.; Liu, X.H. Establishing the first hidden-charm pentaquark with strangeness. *Eur. Phys. J. C* **2021**, *81*, 409. [CrossRef]
15. Azizi, K.; Sarac, Y.; Sundu, H. Investigation of the strange pentaquark candidate $P_{\psi s}^\Lambda(4338)^0$ recently observed by LHCb. *arXiv* **2023**, arXiv:2304.00604.
16. Ortega, P.G.; Entem, D.R.; Fernandez, F. Strange hidden-charm PψsΛ(4459) and PψsΛ(4338) pentaquarks and additional PψsΛ, PψsΣ and PψssN candidates in a quark model approach. *Phys. Lett. B* **2023**, *838*, 137747. [CrossRef]
17. Giachino, A.; Hosaka, A.; Santopinto, E.; Takeuchi, S.; Takizawa, M.; Yamaguchi, Y. Rich structure of the hidden-charm pentaquarks near threshold regions. *Phys. Rev. D* **2022**, *108*, 074012. [CrossRef]
18. Yang, Z.Y.; Peng, F.Z.; Yan, M.J.; Sánchez Sánchez, M.; Pavon Valderrama, M. Molecular P_ψ pentaquarks from light-meson exchange saturation. *arXiv* **2022**, arXiv:2211.08211. https://doi.org/10.48550/arXiv.2211.08211.
19. Wang, F.L.; Liu, X. Emergence of molecular-type characteristic spectrum of hidden-charm pentaquark with strangeness embodied in the PψsΛ(4338) and Pcs(4459). *Phys. Lett. B* **2022**, *835*, 137583. [CrossRef]
20. Karliner, M.; Rosner, J.L. New strange pentaquarks. *Phys. Rev. D* **2022**, *106*, 036024. [CrossRef]
21. Meng, L.; Wang, B.; Zhu, S.L. Double thresholds distort the line shapes of the PψsΛ(4338)0 resonance. *Phys. Rev. D* **2023**, *107*, 014005. https://doi.org/10.1103/PhysRevD.107.014005.
22. Shi, P.P.; Huang, F.; Wang, W.L. Hidden charm pentaquark states in a diquark model. *Eur. Phys. J. A* **2021**, *57*, 237. [CrossRef]
23. Xiao, C.W.; Wu, J.J.; Zou, B.S. Molecular nature of $P_{cs}(4459)$ and its heavy quark spin partners. *Phys. Rev. D* **2021**, *103*, 054016. [CrossRef]

24. Chen, R. Can the newly reported $P_{cs}(4459)$ be a strange hidden-charm $\Xi_c\bar{D}^*$ molecular pentaquark? *Phys. Rev. D* **2021**, *103*, 054007. [CrossRef]
25. Chen, K.; Lin, Z.Y.; Zhu, S.L. Comparison between the PψN and PψsΛ systems. *Phys. Rev. D* **2022**, *106*, 116017. [CrossRef]
26. Li, S.Y.; Liu, Y.R.; Man, Z.L.; Si, Z.G.; Wu, J. Hidden-charm pentaquark states in a mass splitting model. *Phys. Rev. D* **2023**, *108*, 056015. [CrossRef]
27. Maiani, L.; Polosa, A.D.; Riquer, V. The pentaquark spectrum from Fermi statistics. *Eur. Phys. J. C* **2023**, *83*, 378. [CrossRef]
28. Burns, T.J.; Swanson, E.S. The LHCb state PψsΛ(4338) as a triangle singularity. *Phys. Lett. B* **2023**, *838*, 137715. [CrossRef]
29. Ke, H.W.; Lu, F.; Pang, H.; Liu, X.H.; Li, X.Q. Study on the possible molecular states composed of $\Lambda_c\bar{D}^*$, $\Sigma_c\bar{D}^*$, $\Xi_c\bar{D}^*$ and $\Xi'_c\bar{D}^*$ in the Bethe-Salpeter frame based on the pentaquark states $P_c(4440)$, $P_c(4457)$ and $P_{cs}(4459)$. *arXiv* **2023**, arXiv:2308.00582. https://doi.org/10.48550/arXiv.2308.00582.
30. Yalikun, N.; Dong, X.K.; Zou, B.S. Molecular states in $D_s^{(*)+}\Xi_c^{(',*)}$ systems. *arXiv* **2023**, arXiv:2303.03629. https://doi.org/10.1088/1674-1137/acf65e.
31. Wu, T.W.; Pan, Y.W.; Liu, M.Z.; Lu, J.X.; Geng, L.S.; Liu, X.H. Hidden charm hadronic molecule with strangeness Pcs*(4739) as a ΣcD$^-$K$^-$ bound state. *Phys. Rev. D* **2021**, *104*, 094032. [CrossRef]
32. Wang, F.L.; Liu, X. Higher molecular PψsΛ/Σ pentaquarks arising from the Ξc(',*)D$^-$1/Ξc(',*)D$^-$2* interactions. *Phys. Rev. D* **2023**, *108*, 054028. [CrossRef]
33. Ozdem, U. Electromagnetic properties of $\bar{D}^{(*)}\Xi'_c$, $\bar{D}^{(*)}\Lambda_c$, $\bar{D}_s^{(*)}\Lambda_c$ and $\bar{D}_s^{(*)}\Xi_c$ pentaquarks. *arXiv* **2023**, arXiv:2303.10649. https://doi.org/10.48550/arXiv.2303.10649.
34. Wang, F.L.; Zhou, H.Y.; Liu, Z.W.; Liu, X. What can we learn from the electromagnetic properties of hidden-charm molecular pentaquarks with single strangeness? *Phys. Rev. D* **2022**, *106*, 054020. [CrossRef]
35. Özdem, U. Investigation of magnetic moment of Pcs(4338) and Pcs(4459) pentaquark states. *Phys. Lett. B* **2023**, *836*, 137635. [CrossRef]
36. Li, M.W.; Liu, Z.W.; Sun, Z.F.; Chen, R. Magnetic moments and transition magnetic moments of Pc and Pcs states. *Phys. Rev. D* **2021**, *104*, 054016. [CrossRef]
37. Paryev, E.Y. On the possibility of testing the two-peak structure of the LHCb hidden-charm strange pentaquark Pcs(4459)0 in near-threshold antikaon-induced charmonium production on protons and nuclei. *Nucl. Phys. A* **2023**, *1037*, 122687. [CrossRef]
38. Cheng, C.; Yang, F.; Huang, Y. Searching for strange hidden-charm pentaquark state Pcs(4459) in γp$\rightarrow$K+Pcs(4459) reaction. *Phys. Rev. D* **2021**, *104*, 116007. [CrossRef]
39. Yang, F.; Huang, Y.; Zhu, H.Q. Strong decays of the $P_{cs}(4459)$ as a $\Xi_c\bar{D}^*$ molecule. *Sci. China Phys. Mech. Astron.* **2021**, *64*, 121011. [CrossRef]
40. Chen, R. Strong decays of the newly $P_{cs}(4459)$ as a strange hidden-charm $\Xi_c\bar{D}^*$ molecule. *Eur. Phys. J. C* **2021**, *81*, 122. [CrossRef]
41. Azizi, K.; Sarac, Y.; Sundu, H. Investigation of $P_{cs}(4459)^0$ pentaquark via its strong decay to $\Lambda J/\Psi$. *Phys. Rev. D* **2021**, *103*, 094033. [CrossRef]
42. Liu, W.Y.; Hao, W.; Wang, G.Y.; Wang, Y.Y.; Wang, E.; Li, D.M. Resonances $X(4140)$, $X(4160)$, and $P_{cs}(4459)$ in the decay of $\Lambda_b \rightarrow J/\psi\Lambda\phi$. *Phys. Rev. D* **2021**, *103*, 034019. [CrossRef]
43. Wu, Q.; Chen, D.Y.; Ji, R. Production of $P_{cs}(4459)$ from Ξ_b Decay. *Chin. Phys. Lett.* **2021**, *38*, 071301. [CrossRef]
44. Lu, J.X.; Liu, M.Z.; Shi, R.X.; Geng, L.S. Understanding Pcs(4459) as a hadronic molecule in the Ξb-$\rightarrow$J/$\psi\Lambda$K- decay. *Phys. Rev. D* **2021**, *104*, 034022. [CrossRef]
45. Vijande, J.; Fernandez, F.; Valcarce, A. Constituent quark model study of the meson spectra. *J. Phys. G* **2005**, *31*, 481. [CrossRef]
46. Segovia, J.; Entem, D.R.; Fernandez, F.; Hernandez, E. Constituent quark model description of charmonium phenomenology. *Int. J. Mod. Phys.* **2013**, *E22*, 1330026. [CrossRef]
47. Hiyama, E.; Kino, Y.; Kamimura, M. Gaussian expansion method for few-body systems. *Prog. Part. Nucl. Phys.* **2003**, *51*, 223–307. [CrossRef]
48. Myo, T.; Kikuchi, Y.; Masui, H.; Katō, K. Recent development of complex scaling method for many-body resonances and continua in light nuclei. *Prog. Part. Nucl. Phys.* **2014**, *79*, 1–56. [CrossRef]
49. Yang, G.; Ping, J.; Segovia, J. Tetra- and penta-quark structures in the constituent quark model. *Symmetry* **2020**, *12*, 1869. [CrossRef]
50. Yang, G.; Ping, J.; Segovia, J. Charmoniumlike tetraquarks in a chiral quark model. *Eur. Phys. J. C* **2023**, *83*, 772. [CrossRef]
51. Yang, G.; Ping, J.; Segovia, J. Exotic resonances of fully-heavy tetraquarks in a lattice-QCD insipired quark model. *Phys. Rev. D* **2021**, *104*, 014006. [CrossRef]
52. Yang, G.; Ping, J.; Segovia, J. Fully charm and bottom pentaquarks in a lattice-QCD inspired quark model. *Phys. Rev. D* **2022**, *106*, 014005. [CrossRef]
53. Aguilar, J.; Combes, J.M. A class of analytic perturbations for one-body Schrödinger Hamiltonians. *Commun. Math. Phys.* **1971**, *22*, 269. [CrossRef]
54. Balslev, E.; Combes, J.M. Spectral properties of many-body Schrödinger operators with dilatation-analytic interactions. *Commun. Math. Phys.* **1971**, *22*, 280. [CrossRef]
55. Bali, G.S.; Neff, H.; Duessel, T.; Lippert, T.; Schilling, K. Observation of string breaking in QCD. *Phys. Rev.* **2005**, *D71*, 114513. [CrossRef]
56. Scadron, M.D. Spontaneous breakdown and the scalar nonet. *Phys. Rev. D* **1982**, *26*, 239–247. [CrossRef]

57. Segovia, J.; Entem, D.R.; Fernandez, F. Charmed-strange Meson Spectrum: Old and New Problems. *Phys. Rev. D* **2015**, *91*, 094020. [CrossRef]
58. Ortega, P.G.; Segovia, J.; Entem, D.R.; Fernandez, F. Spectroscopy of **B$_c$** mesons and the possibility of finding exotic **B$_c$**-like structures. *Eur. Phys. J. C* **2020**, *80*, 223. [CrossRef]
59. Yang, G.; Ping, J.; Segovia, J. The S- and P-Wave Low-Lying Baryons in the Chiral Quark Model. *Few Body Syst.* **2018**, *59*, 113. [CrossRef]
60. Segovia, J.; Entem, D.R.; Fernandez, F. Charmonium resonances in e+ e- exclusive reactions around the psi(4415) region. *Phys. Rev. D* **2011**, *83*, 114018. [CrossRef]
61. Ortega, P.G.; Segovia, J.; Entem, D.R.; Fernández, F. Threshold effects in P-wave bottom-strange mesons. *Phys. Rev.* **2017**, *D95*, 034010. [CrossRef]
62. Ortega, P.G.; Segovia, J.; Entem, D.R.; Fernández, F. The Z_c structures in a coupled-channels model. *Eur. Phys. J. C* **2019**, *79*, 78. [CrossRef]
63. Harvey, M. Effective nuclear forces in the quark model with Delta and hidden color channel coupling. *Nucl. Phys.* **1981**, *A352*, 326–342. [CrossRef]
64. Vijande, J.; Valcarce, A.; Barnea, N. Exotic meson-meson molecules and compact four–quark states. *Phys. Rev. D* **2009**, *79*, 074010. [CrossRef]
65. Yang, G.; Ping, J. The structure of pentaquarks P_c^+ in the chiral quark model. *Phys. Rev. D* **2017**, *95*, 014010. [CrossRef]
66. Yang, G.; Ping, J.; Segovia, J. Doubly Charmed Pentaquarks. *Phys. Rev. D* **2020**, *101*, 074030. [CrossRef]
67. Yang, G.; Ping, J.; Segovia, J. Doubly-heavy tetraquarks. *Phys. Rev. D* **2020**, *101*, 014001. [CrossRef]